A New Measurement of the X-ray Temperature Function of Clusters of Galaxies

Yasushi Ikebe[1], Thomas H. Reiprich[2], Hans Böhringer[1], Yasuo Tanaka[1,3] and Tetsu Kitayama[4]

[1] Max-Planck-Institut für extraterrestrische Physik, Postfach 1312, 85741 Garching, Germany
[2] Department of Astronomy, University of Virginia, PO Box 3818, 530 McCormick Road, Charlottesville, VA 22903-0818, USA
[3] Institute of Space and Astronautical Science, Yoshinodai 3-1-1, Sagamihara, Kanagawa 229-8510, Japan
[4] Department of Physics, Toho University, Miyama, Funabashi, Chiba 274-8510, Japan

Abstract. We present a newly measured X-ray temperature function of galaxy clusters using a complete flux-limited sample of 61 clusters. The sample is constructed with the total survey area of 8.14 steradians and the flux limit of 1.99×10^{-11} ergs s^{-1} cm^{-2} in the 0.1–2.4 keV band. X-ray temperatures and fluxes of the sample clusters were accurately measured with *ASCA* and *ROSAT* data. The derived temperature function covers an unprecedentedly wide temperature range of 1.4-11 keV. By fitting these data with theoretically predicted temperature functions given by the Press-Schechter formalism together with a recent formation approximation and the CDM power spectrum, we obtained tight and individual constraints on $\Omega_{m,0}$ and σ_8. We also employed the Formation-Epoch model in which the distribution in the formation epoch of clusters as well as the temperature evolution are taken into account, showing significantly different results. Systematics caused by the uncertainty in the mass-temperature relation are studied and found to be as large as the statistical errors.

Key words. Cosmology: observations — cosmological parameters — X-rays: galaxies: clusters

1. Introduction

The mass function of clusters of galaxies (MF), the number density of the most massive virialized systems, contains information on the structure formation history of the universe. A theoretical framework, e.g. the Press-Schechter formalism (Press & Schechter 1974) together with the Cold Dark Matter model, has been established to predict the MF. This allows us to constrain cosmological parameters using an observationally determined MF for the present epoch (as well as its time evolution for even tighter constraints). In particular, σ_8, the amplitude of mass density fluctuations on a scale of $8h^{-1}$ Mpc where h is the Hubble constant in unit of 100 km/s/Mpc, and $\Omega_{m,0}$, the mean matter density, are most sensitively determined by the cluster abundance measurements (e.g. Henry & Arnaud 1991; White et al. 1993; Eke et al. 1996; Kitayama & Suto 1996; Viana & Liddle 1996; Oukbir & Blanchard 1997; Pen 1998; Eke et al. 1998).

Observationally the local MF has been derived from measuring masses of individual clusters from galaxy velocity dispersions or other optical properties by Bahcall and Cen (1993), Biviano et al. (1993), and Girardi et al. (1998).

The estimated virial masses for individual clusters depend rather strongly on model assumptions, however. As argued by Evrard et al. (1997) on the basis of hydrodynamical N-body simulations, cluster masses may be presently more accurately determined from a temperature measurement and a mass-temperature relation determined from detailed observations or numerical modeling. Thus alternatively, as a well-defined observational quantity, the X-ray temperature function (XTF) has been measured, which can be converted to the MF by means of the mass-temperature relation.

The first measurements of the XTF were reported by Edge et al. (1990) and Henry & Arnaud (1991), using an X-ray flux-limited sample of 45 clusters and 25 clusters, respectively. Recent observational improvement on the XTF was made by Markevitch (1998), Henry (2000), Blanchard et al. (2000), and Pierpaoli et al. (2001), using more accurate temperature-measurement results for each cluster with *ASCA* data (Tanaka et al. 1994). However, the narrow temperature ranges (3-10 keV) in which the XTF is defined so far do not allow an investigation of a more detailed shape of the XTF other than just fitting a single power-law. Without better information on the actual shape of the XTF, no independent constraints on σ_8 and $\Omega_{m,0}$ can be derived, and a wide range of combinations

is still allowed. Recently, a number of new X-ray-cluster surveys were performed, which provide a high completeness for the brightest clusters. This motivated us to revisit the measurement of the local XTF and to improve its accuracy in order to derive narrower constraints on the cosmological parameters.

Reiprich & Böhringer (2002) have compiled a new X-ray flux-limited cluster sample (*HIFLUGCS*) with a flux limit of 2×10^{-11} ergs s^{-1} cm^{-2} (0.1-2.4 keV). Compared with previous samples with similar flux limits, their catalog covers the largest volume and is the most complete. Based on this cluster sample, Reiprich & Böhringer have measured total masses for individual clusters and derived the X-ray mass function for the first time. In this paper we, using this cluster sample, report the construction of a new measurement of the XTF. The larger number of clusters in the sample together with accurate temperature measurements with *ASCA* data leads to a significant improvement of the XTF, which covers 1.4-11 keV temperature range. The X-ray flux-limited sample and the new temperature measurements with *ASCA* data are presented in Sect. 2. The derivation of the XTF is described in Sect. 3. In Sect. 4, the XTF is used to obtain constraints on cosmological parameters, and the results are compared with other work in Sect. 5. Throughout the paper, the Hubble constant is given as 100 h km/s/Mpc, and log and ln denotes a decimal and natural logarithm, respectively.

2. Sample and analysis of *ASCA* data

2.1. Master catalog

For this study we use a sample of 106 galaxy clusters compiled by Reiprich & Böhringer (2002), which is used to construct a flux-limited complete sample (*HIFLUGCS*) with the flux-limit of 2.0×10^{-11} ergs s^{-1} cm^{-2} (0.1-2.4 keV). The 106 clusters have been derived from combining previous X-ray cluster or elliptical galaxy catalogs that include Böhringer et al. (2000, 2001), Böhringer (1999), Retzlaff et al. in preparation, Ebeling et al. (1996, 1998), de Grandi et al. (1999), Beuing et al. (1999), Lahav et al. (1989), and Edge et al. (1990). Most of them are based on the *ROSAT* All Sky Survey (Trümper 1993; Voges et al. 1999). From these catalogs, all objects satisfying certain criteria, mainly that the measured flux given in any of these catalogs is above 1.7×10^{-11} ergs s^{-1} cm^{-2} (0.1-2.4 keV), have been sampled. A defined region around the center of M87 is not included in the survey area, because of the large scale emission of the Virgo cluster that compromises cluster detection and characterization in the region. This excludes the Virgo cluster and M86 from the master catalog. The count rate of the PSPC (Pfeffermann et al. 1987) in the 0.1-2.4 keV band for each object was redetermined from the *ROSAT* All Sky Survey data or PSPC pointing observations whenever available by integrating all X-ray flux within a maximum radius where the cluster emission is significantly detected. See Reiprich & Böhringer (2002) for detailed descriptions of the sample construction and data analysis. The names and the redshifts compiled from the recent literature of all the 106 clusters are listed in Table 1.

As described below, we newly determine the X-ray temperature as well as the X-ray flux for each of the 106 clusters. *ASCA* data are available for 88 of the 106 clusters, and the X-ray temperatures are measured by analyzing the *ASCA* data (Sect. 2.2). Using the *ASCA* results, the correlation between the X-ray luminosity and the temperature, $L - T$ relation, is established (Sect. 2.3). Among the other clusters for which no *ASCA* data exist (18 clusters), temperatures of 4 clusters have been measured with *Einstein*, *EXOSAT*, or *XMM-Newton* in previous works and were used in our analysis. For the remaining 14 clusters, the temperatures are estimated from the observed *ROSAT* PSPC count rate by means of the $L - T$ relation. By setting a flux-limit of 1.99×10^{-11} ergs s^{-1} cm^{-2} (0.1-2.4 keV), a complete flux-limited sample comprising 63 clusters is then constructed (Sect. 2.4).

2.2. Temperature Measurements

For our study we need to determine an average temperature for each cluster that closely reflects the mass of the cluster, i.e. a virial temperature. In many clusters, the X-ray emitting hot gas is not isothermal but a cooler gas component is often observed in the central region. The cool component, which is due to either a cooling flow (e.g. Fabian 1994) or the ISM of cD galaxies (e.g. Makishima et al. 2001), often exhibits a significant fraction of the luminosity and has to be separated from the rest of the X-ray emission to determine the cluster average temperature (see also Markevitch 1998; Arnaud & Evrard 1999).

Therefore, in the *ASCA* data analysis, we employed a two-temperature (2T) model, in which isothermal plasma is filling the entire cluster region, while, in the central region, another cooler isothermal gas component is allowed to coexist with the hotter plasma forming a multiphase intra-cluster medium (ICM). This 2T picture was established for the Centaurus cluster (Fukazawa et al. 1994; Ikebe et al. 1999) and also gave a good account of the *ASCA* data of Virgo/M87 (Matsumoto et al. 1996), Hydra-A (Ikebe et al. 1997), Abell 1795 (Xu et al. 1998), and other nearby clusters (Fukazawa 1997; Fukazawa et al. 1998, 2000). The hot component extends over the major part of cluster volume as far as is measurable (e.g. Fukazawa 1997; White 2000). The temperature of this hot component derived from the 2T model therefore represents the best estimation of the virial temperature of the cluster. Although a cooling flow spectral model also gives generally a good description of the *ASCA* spectra (e.g. Fabian et al. 1994; White 2000; Allen et al. 2001), the estimated temperatures from where gas starts to cool vary considerably from author to author and are sometimes spuriously high. More importantly, recent *XMM-Newton* data clearly show that the conventional cooling flow spectral model is not adequate (Peterson et al. 2001; Tamura et al. 2001;

Kaastra et al. 2001). The 2T model, on the other hand, is valid to the *XMM-Newton* data and the hot component temperature well represents the temperature of the outer main component (see Ikebe 2001).

It is known that, apart from the central cool component, many clusters show deviations from isothermality such as an asymmetric temperature distribution due to merging (e.g. Briel & Henry 1994) or a global temperature decrement towards the outside (Markevitch et al. 1998). For such clusters, the 2T model fit gives insignificant flux to the cool component and works practically as an isothermal model. Thus the hot component temperature gives the average temperature, which also can be a good measure of the virial temperature.

Among the 106 sample clusters, 88 clusters have been observed with *ASCA*, and all the data sets have become publicly available by now. We retrieved the *ASCA* data from the *ASCA* archival data base provided by NASA Goddard Space Flight Center and by Leicester University. Here we will give a brief explanation of the analysis method of the *ASCA* data.

ASCA has four focal plane instruments, two SIS (Solid-state Imaging Spectrometer) and two GIS (Gas Imaging Spectrometer; Ohashi et al. 1996), which were usually used simultaneously to observe an astronomical object. In all the observations, the GIS were operated in the normal PH mode and the SIS were operated in FAINT mode or BRIGHT mode. The number of active CCD chips of each SIS used was 4, 2, or 1, corresponding to the field of view of $22' \times 22'$, $22' \times 11'$, or $11' \times 11'$, respectively.

We discarded the GIS and SIS data that were taken when the elevation angle of the X-Ray Telescope (XRT) from the local horizon was less than $5°$. An additional screening requirement, that the elevation angle from the sunlit earth be greater than $25°$ and $20°$, was applied to the SIS-0 and SIS-1 data, respectively. In order to ensure a low and stable particle background, we also discarded GIS and SIS data acquired under a geomagnetic cutoff rigidity smaller than 6 GV.

The background is composed of cosmic X-ray background and non-X-ray background, which were estimated for each cluster observation from the data of blank-sky observations as well as the data taken when the X-Ray Telescope was pointing at the dark (night) earth.

In order to maximize the detection efficiency of the central cool component, we accumulated spectra over two regions, a central region of $2'$ radius and an outer region from $2'$ to r_{max}, from each cluster data set. r_{max}, the maximum radius, is defined as the radius within which at least 95% of all detected source X-ray counts, within the field of view of the GIS, are included. The data from the two GIS sensors and two SIS sensors were combined. Thus for each cluster, four spectra: two central and two outer spectra for GIS and SIS, were derived.

An effective area as a function of X-ray energy was calculated for each spectrum with an *ASCA* simulator (SimARF). The point-spread-function of the *ASCA* XRT is so largely extended that the X-ray flux from the central

brightest region may contribute to the outer region spectrum (Serlemitsos et al. 1995; Takahashi et al. 1995). We therefore, simultaneously fitted the four spectra with the 2T model, taking into account the flux-contamination effect. As a plasma code, we used the MEKAL model (Mewe et al. 1985, 1986; Kaastra 1992, Liedahl et al. 1995), that is implemented in XSPEC version 10.0 (Arnaud 1996).

A best-fit model was derived by a chi-square minimization method. The cool and hot component temperatures are separate free parameters. Many clusters do not require an additional cool component to fit the spectra, and the cool component temperatures cannot be constrained. For each cluster we investigated the significance of adding a cool component by comparison with a fit of a hot isothermal model and performing an F-test. For a cluster showing a low significance for the additional cool component in the 2T model, we fixed the temperature of the cool component at $T_{iso}/2$, where T_{iso} is the temperature derived with the isothermal model fitting. The choice of the fixed cool-component temperature is based on a clear correlation found in the 2T model fitting that, for clusters showing a high significance for the cool component, the cool-component temperature is always very close to half of the hot component temperature (see Ikebe 2001). The hot component temperatures thus derived are summarized in Table 1. A more detailed analysis procedure description and results on the cool components will be presented in a following publication.

We compared the temperatures derived here with those of previous workers. The temperatures agree with results of Fukazawa (1997) within 1.5% on average (Fig. 1a), who performed a similar analysis on a smaller number of clusters with *ASCA* data, accumulating spectra from a central region of 2-3 arc-minutes radius and an outer region, and fitting them with the 2T model. On the other hand, temperatures given by Markevitch et al. (1998) and White (2000), who used different (cooling flow) models to fit the *ASCA* spectra, are higher than our values respectively by a factor of 1.09 and 1.25 on average for clusters hotter than 6 keV (Fig. 1b,c). This difference causes a significant difference in the resulting XTFs (see Sect. 3.2).

2.3. $L - T$ relation

For the 88 clusters observed with *ASCA*, X-ray fluxes and luminosities were calculated from the spectral-analysis results described above and the *ROSAT* PSPC count rates in 50-201 PI channel given by Reiprich & Böhringer (2002). Assuming isothermality in each cluster at the hot-component temperature and the Galactic column density given in Table 1, we determined the 0.1–2.4 keV fluxes and luminosities that reproduce the PSPC count rates. As summarized in Table 1, the luminosities were calculated for two different cosmological models with an open $(\Omega_{m,0} = 0.2, \Omega_{\Lambda,0} = 0)$ and a flat $(\Omega_{m,0} = 0.2, \Omega_{\Lambda,0} = 0.8)$ universe.
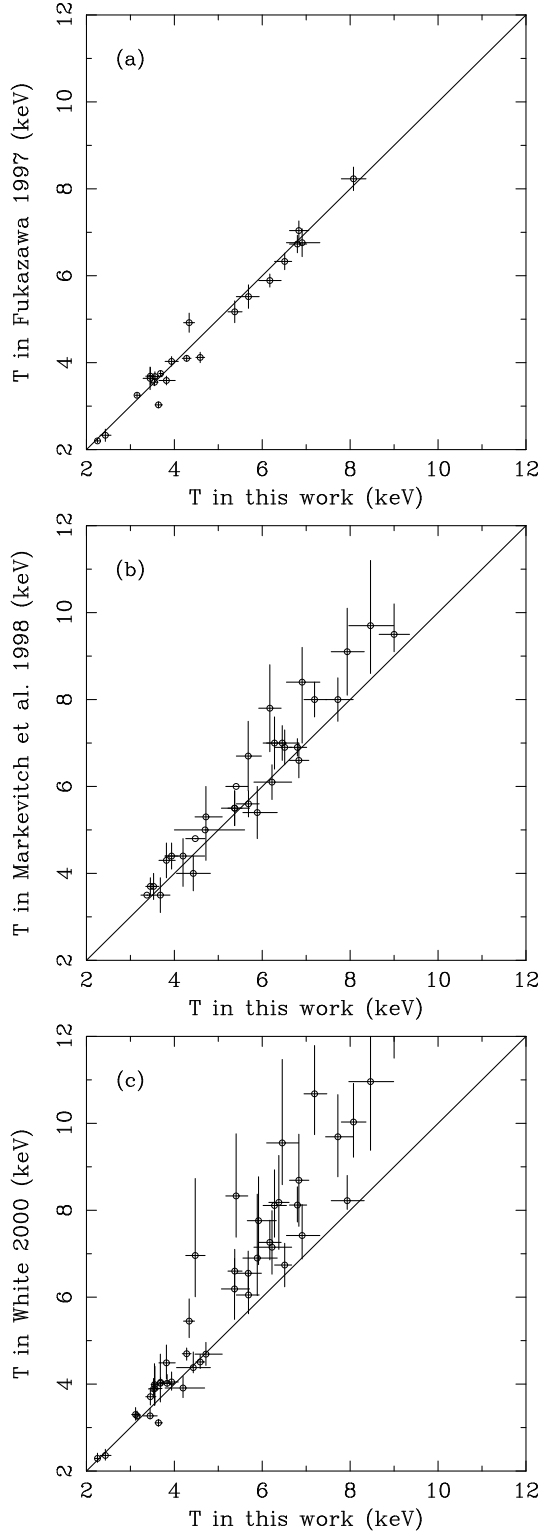
Fig. 1. Comparison between the cluster temperatures derived here and those by Fukazawa (1997) (a), by Markevitch et al. (1998) (b), and by White (2000) (c).

We then established a correlation between the luminosity in the 0.1–2.4 keV band, $L_{0.1-2.4\text{keV}}$, and the temperature of the hot component, T_h, as illustrated in Fig. 2. The $L_{0.1-2.4\text{keV}}$-T_h relations for the open and flat universe
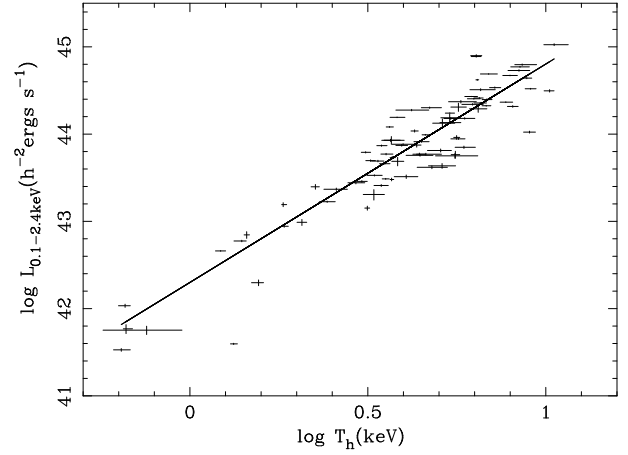

Fig. 2. The luminosities in the energy range of 0.1-2.4 keV in the cluster rest frame in a flat universe ($\Omega_{m,0} = 0.2$, $\Omega_{\Lambda,0} = 0.8$) as a function of the hot component temperature obtained from the two-temperature model fitted to the *ASCA* data. The best-fit power-law function (eq. 2) is overlayed.

were fitted individually with power-law functions by a linear regression method. For the fit we did not use clusters with a hot component temperature cooler than 1.4 keV, because it is known that a single power-law function is not a good representation of the $L - T$ relation over a wide temperature range. In particular, including clusters, groups, and elliptical galaxies, the $L - T$ relation becomes steeper below ~ 1 keV (e.g. Xue & Wu 2000). Moreover, the theoretically predicted XTFs as given in Sect. 4 may not be directly compared with an observed XTF (see Sect. 4.3 for more explanation). Therefore, in the power-law fitting, we exclude 6 sample clusters cooler than 1.4 keV and use only 82 clusters. For the linear regression fit, we employed the BCES($X_2|X_1$) estimator given by Akritas & Bershady (1996) (In this case, the luminosity and temperature are assigned as X_2 and X_1, respectively). The choice of the estimator is based on an argument by Isobe et al. (1990). The best-fit functions are

$$\log L_{0.1-2.4\text{keV}}(h^{-2}\text{ergs s}^{-1}) =$$
$$42.31\,(\pm0.09) + 2.47\,(\pm0.14)\,\log T_h(\text{keV}) \qquad (1)$$

for the open universe, and

$$\log L_{0.1-2.4\text{keV}}(h^{-2}\text{ergs s}^{-1}) =$$
$$42.30\,(\pm0.09) + 2.50\,(\pm0.14)\,\log T_h(\text{keV}) \qquad (2)$$

for the flat universe.

We have made a correction to the derived $L_{0.1-2.4\text{keV}} - T_h$ relation. Since the less luminous clusters are less likely to be sampled, the apparent *mean* luminosity at a given temperature, which is estimated by the simple regression fit, is biased towards higher values than the true mean value. As will be shown in Sect. 4, we studied this effect and corrected the normalization to derive the "true" $L_{0.1-2.4\text{keV}} - T_h$ relation, as

$$\log L_{0.1-2.4\text{keV}}(h^{-2}\text{ergs s}^{-1}) = 42.15 + 2.47\,\log T_h(\text{keV}) \qquad (3)$$

for the open universe, and

$$\log L_{0.1-2.4\text{keV}}(h^{-2}\text{ergs s}^{-1}) = 42.14 + 2.50 \log T_{\text{h}}(\text{keV}) \quad (4)$$

for the flat universe. The correction reduces the luminosity at a given temperature by 30%. The corrected $L_{0.1-2.4\text{keV}} - T_{\text{h}}$ relation will also be used to calculate V_{max} in Sect. 3. The 30% reduction of the mean temperature results in a reduction of V_{max} (see Sect. 3) by 40%.

Using the corrected $L_{0.1-2.4\text{keV}} - T_{\text{h}}$ relations, we estimated the temperatures of 14 clusters for which no *ASCA* data nor other spectroscopic measurement are available. An $L_{0.1-2.4\text{keV}}$ and T_{h} combination was chosen from the $L_{0.1-2.4\text{keV}} - T_{\text{h}}$ relation such that the predicted PSPC count rate equals the observed value. Scatter around the best-fit power-law in the $L-T$ relation was assigned as error. The estimated temperatures and luminosities for the open and flat universe cases as well as the corresponding 0.1–2.4 keV fluxes which are the same for the open and flat universe cases are summarized in Table 1.

2.4. Construction of the flux limited sample

We set a flux-limit of 1.99×10^{-11} ergs s^{-1} cm^{-2} in 0.1–2.4 keV band to construct a flux-limited complete sample from the master catalog of 106 clusters. As in Reiprich & Böhringer (2002) for *HIFLUGCS*, additional selection criteria applied are that the absolute Galactic latitude is greater than 20°, and the cluster is located neither in the Magellanic Clouds nor in the Virgo cluster region. The total number of clusters thus selected is 63, whose temperatures and redshifts are shown in Fig. 3. Since the temperatures of the individual clusters were newly determined in this paper, the fluxes estimated from the PSPC count rate are slightly revised from the value in Reiprich & Böhringer (2002) where the temperatures are compiled from literature. All of the 63 clusters selected here, however, still correspond with the 63 *HIFLUGCS* clusters. Tests performed in Reiprich & Böhringer (2002) showed no indication of incompleteness of the sample.

In the following analysis, we exclude 2 clusters cooler than 1.4 keV (see Sect. 2.3 and 4.3) from the flux-limited complete sample, and use 61 clusters to study the XTF and make constraints on cosmological parameters. This is the largest complete sample of clusters up to now with temperature measurements or reliable temperature estimates. We also stress the accuracy of the temperature measurements for the sample clusters: Among the 61 clusters used for constructing the XTF, the temperatures of 56 clusters (90% of the sample) were measured with *ASCA* data with 90% errors of 6-10%, other spectroscopic measurements were used for 3 clusters, and there are only two clusters for which the temperature is estimated with the $L-T$ relation.
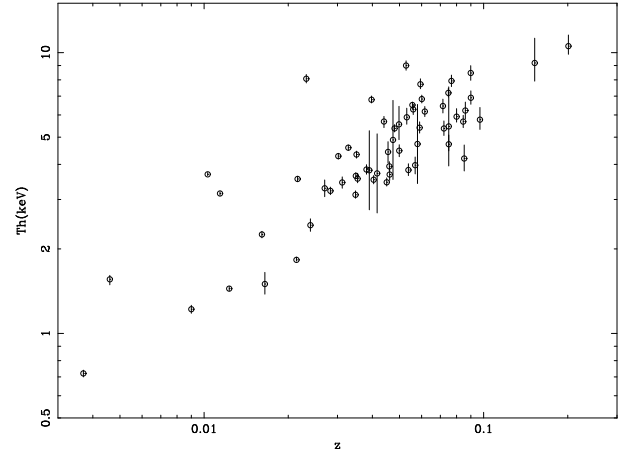
3. The Temperature Function

Fig. 3. X-ray temperature vs redshift for the clusters of the flux-limited sample.

3.1. Derivation of XTF

Using the X-ray flux-limited complete sample of 61 clusters ($T_{\text{h}} \geq 1.4$), we address in this section the XTF describing the number density of clusters of galaxies in comoving coordinates at present as a function of the X-ray temperature. A full description of the analysis method can be found in the Appendix. However, the key points are presented here. The differential temperature function, $\phi(T)$, is defined as the number density of clusters in the temperature range from $T - \frac{dT}{2}$ to $T + \frac{dT}{2}$. From a finite number of sample clusters, it can be evaluated as

$$\phi(T)dT = \sum_{T - \frac{\Delta T}{2} \leq T_{\text{i}} < T + \frac{\Delta T}{2}} \frac{1}{V_{\text{max}}(T_{\text{i}})} \quad (5)$$

where i denotes a sequential number of clusters in a temperature range from $T - \frac{\Delta T}{2}$ to $T + \frac{\Delta T}{2}$, and $V_{\text{max}}(T_{\text{i}})$ is a maximum comoving volume in which a cluster having a temperature of T_{i} could have been detected under the selection criteria given above. Following Markevitch (1998), we assume, for a given temperature, the logarithmic luminosity, $\log L$, follows a Gaussian distribution around the mean which is given with the $L-T$ relation, i.e. $L = AT^{\alpha}$, and with a constant standard deviation of $\sigma_{\log L}$. $V_{\text{max}}(T)$ then can be evaluated as

$$V_{\text{max}}(T) =$$
$$\int_{-\infty}^{\infty} \frac{v_{\text{max}}(L,T)}{\sqrt{2\pi\sigma_{\log L}^2}} \exp\left\{-\frac{(\log AT^{\alpha} - \log L)^2}{2\sigma_{\log L}^2}\right\} d\log L, \quad (6)$$

where $v_{\text{max}}(L,T)$ is the maximum search volume for a cluster having the luminosity of L and the temperature of T and is given by Eq. A.9. Recall that $V_{\text{max}}(T)$ depends on the cosmological parameters and was calculated for an open ($\Omega_{\text{m},0} = 0.2, \Omega_{\Lambda,0} = 0$) and a flat ($\Omega_{\text{m},0} = 0.2, \Omega_{\Lambda,0} = 0.8$) universe. The results are listed for individual clusters in Table 2. The XTF thus derived with 1 keV bin widths is illustrated in Fig. 4.

The improvement of the new result over previous work is mainly characterized by a significant broadening of
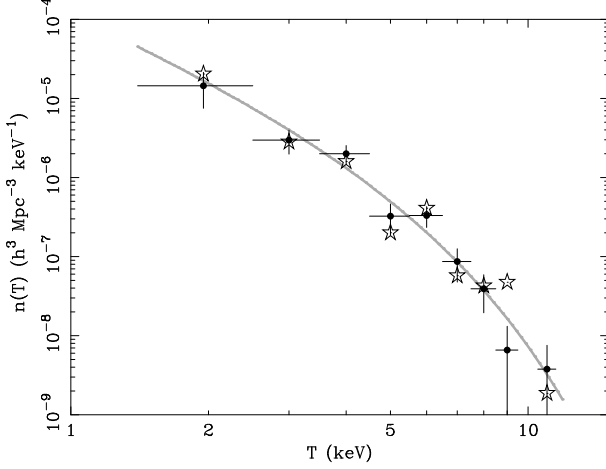
Fig. 4. The X-ray temperature function derived with the flux-limited complete sample of 61 clusters for the case of a flat universe ($\Omega_{m,0} = 0.2, \Omega_{\Lambda,0} = 0.8$). Filled circles show the XTF evaluated with $1/V_{max}(T_i)$, while open stars show the one obtained with $1/v_{max}(L_i, T_i)$. The temperature bin widths are 1 keV, except for the lowest temperature bin that includes kT=1.4–2.5 keV. The vertical error bars for filled circles indicate Poisson errors. Open stars should have the same Poisson errors, which are omitted for a clear display. The solid curve is the best-fit Press-Schechter function derived in Sect. 4.1.

the temperature range towards lower temperature systems down to 1.4 keV. A single power law is no longer a good description to the observationally measured XTF and an exponential cut off towards the higher temperature is clearly seen, as a theoretical model predicts. The detection of such a curvature brings tight constraints on cosmological parameters as will be shown in the next section.

Conventionally, $V_{max}(T_i)$ in Eq. 5 is often simply replaced by $v_{max}(L_i, T_i)$ to evaluate the XTF (e.g. Henry 2000). For comparison, the XTF evaluated with $\phi(T)dT = \sum 1/v_{max}(L_i, T_i)$ is also overlaid in Fig. 4, which overall shows good agreement with the one with $\sum 1/V_{max}(T_i)$, but exhibits larger variance due to the intrinsic scatter in the $L - T$ relation.

3.2. Comparison to previous results

In Fig. 5, we compare our result to previously obtained XTFs overlaid in the form of best-fit power law functions. In the $3 - 8$ keV range, our XTF shows good agreement with the previous results.

We have derived a cumulative XTF, which is the number density of clusters that are hotter than a certain temperature, by

$$n(T) = \sum_{T < T_i} \frac{1}{V_{max}(T_i)} \ . \tag{7}$$

The resulting cumulative XTF is illustrated in Fig. 6 together with other recent results by Henry (2000) and

Table 2. Summary of the flux-limited complete sample

NAME	kT_h(keV)		[†]$V_{max}(h^{-3}$ Mpc$^{-3})$	
			Open	Flat
A2163	10.55		2.39e+08	2.65e+08
A0754	9.00		1.40e+08	1.52e+08
A2142	8.46		1.14e+08	1.23e+08
COMA	8.07		9.69e+07	1.04e+08
A2029	7.93		9.12e+07	9.78e+07
A3266	7.72		8.30e+07	8.89e+07
A0401	7.19		6.50e+07	6.91e+07
A0478	6.91		5.66e+07	6.00e+07
A2256	6.83		5.45e+07	5.77e+07
A3571	6.80		5.36e+07	5.67e+07
A0085	6.51		4.60e+07	4.87e+07
A0399	6.46		4.46e+07	4.72e+07
A2204	6.38		4.28e+07	4.52e+07
ZwCl1215	[♭] 6.30	[♯] 6.36	4.09e+07	4.49e+07
A3667	6.28		4.05e+07	4.28e+07
A1651	6.22		3.92e+07	4.14e+07
A1795	6.17		3.81e+07	4.02e+07
A2255	5.92		3.29e+07	3.46e+07
A3391	5.89		3.23e+07	3.40e+07
A2244	5.77		3.01e+07	3.17e+07
A0119	5.69		2.86e+07	3.00e+07
A1650	5.68		2.85e+07	2.99e+07
A3395s	5.55		2.64e+07	2.76e+07
A3158	5.41		2.40e+07	2.50e+07
A2065	5.37		2.34e+07	2.44e+07
A3558	5.37		2.35e+07	2.45e+07
A3112	4.72		1.48e+07	1.53e+07
A1644	[♮] 4.70		1.46e+07	1.51e+07
A0496	4.59		1.34e+07	1.39e+07
A3562	4.47		1.22e+07	1.27e+07
A3376	4.43		1.18e+07	1.22e+07
A2147	4.34		1.10e+07	1.13e+07
A2199	4.28		1.04e+07	1.08e+07
A2597	4.20		9.75e+06	1.01e+07
A0133	3.97		8.02e+06	8.25e+06
A4059	3.94		7.76e+06	7.98e+06
A0576	3.83		7.07e+06	7.26e+06
HYDRA-A	3.82		6.98e+06	7.16e+06
A3526	3.69		6.15e+06	6.30e+06
A1736	3.68		6.11e+06	6.26e+06
2A0335	3.64		5.87e+06	6.00e+06
A2063	3.56		5.41e+06	5.53e+06
A1367	3.55		5.36e+06	5.48e+06
A2657	3.53		5.25e+06	5.36e+06
A2634	3.45		4.84e+06	4.94e+06
MKW3S	3.45		4.87e+06	4.97e+06
A2589	3.38		4.48e+06	4.57e+06
MKW8	3.29		4.08e+06	4.16e+06
A4038	3.22		3.78e+06	3.85e+06
A1060	3.15		3.50e+06	3.56e+06
A2052	3.12		3.37e+06	3.43e+06
IIIZw54	[♭] 2.98	[♯] 3.00	2.87e+06	2.99e+06
EXO0422	[♮] 2.90		2.60e+06	2.63e+06
S1101	[♮] 2.60		1.76e+06	1.77e+06
A0400	2.43		1.37e+06	1.38e+06

Table 2. continued

NAME	$kT_{\rm h}$(keV)	$^{\dagger)}V_{\rm max}(h^{-3}\ {\rm Mpc}^{-3})$	
		Open	Flat
A0262	2.25	1.04e+06	1.04e+06
MKW4	1.84	5.00e+05	4.96e+05
A3581	1.83	4.88e+05	4.84e+05
FORNAX	1.56	2.72e+05	2.68e+05
N1550	1.44	2.05e+05	2.02e+05
N507	1.40	1.83e+05	1.79e+05
N5044	1.22	1.10e+05	1.08e+05
N4636	0.66	1.16e+04	1.10e+04

$^{\dagger)},^{\flat)},^{\sharp)},^{\natural)}$: as Table 1.

Fig. 5. The X-ray temperature function derived with the flux-limited complete sample of 61 clusters for the case of a flat universe ($\Omega_{\rm m,0} = 0.2, \Omega_{\Lambda,0} = 0.8$). The three lines indicate previous measurements in the form of the best-fit power-law functions. Solid, dotted, and dashed lines correspond to the results by Markevitch (1998), Edge et al. (1990), and Henry (2000), respectively.

Markevitch (1998). Our result shows agreement with Henry's XTF constructed from his sample of 25 clusters. The individual temperatures of the 25 clusters were evaluated by averaging the previous temperature measurements with *ASCA* and other missions based on single-temperature fits (see Henry 2000), which agree with the hot component temperatures obtained in this work on average within 1%. Above 6 keV, there is apparent disagreement between our result and the result by Markevitch (1998) showing a higher amplitude. This is due to a larger number of clusters in the highest temperature bins in the Markevitch sample, despite the fact that smaller $V_{\rm max}$ values apply to his sample. (Markevitch selected his sample with the same flux limit as ours but also limited the redshift range to $0.04 \le z \le 0.09$). The larger number of very hot clusters in Markevitch (1998) is due to higher temperature estimates compared to our values for temperatures above ~ 6 keV (Fig. 1b).

Blanchard et al. (2000), using a sample and temperatures mainly from the XBACS (Ebeling et al. 1996) and the *ASCA* measurement by Markevitch et al. (1998), respectively, obtained the XTF, which virtually perfectly agrees with that by Markevitch (1998). Pierpaoli et al. (2001), who have made another attempt to derive the XTF, used the same sample as Markevitch (1998) but the temperatures given by White (2000). The Pierpaoli cumulative XTF has the highest amplitude among other works. This is because of the systematically higher temperatures by White (2000) (see Fig. 1).

4. Constraint on cosmological parameters

In the following, using the flux-limited complete sample of 61 clusters ($T_{\rm h} \ge 1.4$) and theoretical XTF models, we obtain constraints on cosmological parameters. The XTF at the present epoch is most sensitive to the amplitude of density fluctuations on a scale of $8h^{-1}$ Mpc, σ_8, and least sensitive to the cosmological constant, Λ. We therefore concentrate on two different $\Omega_{\Lambda,0}$ model families including open ($\Omega_{\rm m,0} < 1$, $\Omega_{\Lambda,0} = 0$) and flat ($\Omega_{\rm m,0} + \Omega_{\Lambda,0} = 1$) universes. Recent measurements of high-redshift SN Ia indicate a positive cosmological constant (Perlmutter et al.
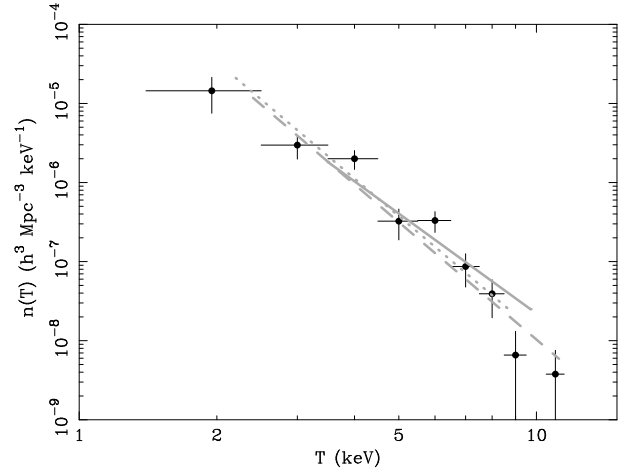

Fig. 6. The cumulative temperature function for the case of a flat universe ($\Omega_{\rm m,0} = 0.2, \Omega_{\Lambda,0} = 0.8$) is shown in grey solid line with its 68% error band. The errors are estimated by $\sqrt{\sum_{T_{\rm i} < T} \left(1/V_{\rm max}(T_{\rm i})\right)^2}$. Previous results from Markevitch (1998) and Henry (2000) are also shown by the solid and dotted black lines, respectively.

1999; Riess et al. 1998). Moreover, the cosmic microwave background (CMB) temperature-fluctuation map recently derived with the Boomerang experiment strongly supports a flat universe model (de Bernardis et al. 2000). Therefore, a flat universe model with a positive cosmological constant is currently the most plausible description of our universe.

For the purpose of comparison with previous works, we also consider the case of an open universe.

For the theoretical prediction of the XTF, we employ two different models, a conventional Press-Schechter mass function (Sect. 4.1) and the Formation-Epoch model by Kitayama & Suto (1996) that is a modification of the former theory (Sect. 4.2). The model XTF depends also on the Hubble constant, which is here assumed to be 71 km/s/Mpc (i.e. $h = 0.71$) based on the latest results of the HST Hubble constant project (see Mould et al. 2000 and references therein).

4.1. Press-Schechter model

According to the Press-Schechter formalism, the number density of clusters with a mass in the range of M to $M + dM$ that have collapsed before a redshift z is given as

$$n_{ps}(M, z)dM =$$
$$\sqrt{\frac{2}{\pi}} \frac{\rho_0}{M} \frac{\delta_c(z)}{\sigma^2(M)} \left|\frac{d\sigma(M)}{dM}\right| \exp\left(-\frac{\delta_c^2(z)}{2\sigma^2(M)}\right) dM , \quad (8)$$

where ρ_0 is the mean density of the universe at present, δ_c is the linear overdensity of a system collapsed at a redshift z and evaluated at present (for which we use the formula given in Kitayama & Suto 1996), and σ^2 is the variance of mass extracted from the density fluctuation field within a spherical region that includes a mass M on average. For the mass variance, we employed an analytical formula derived by Kitayama & Suto (1996) based on the CDM power spectrum, which is given as

$$\sigma \propto (1 + 2.208m^p - 0.7669m^{2p} + 0.7949m^{3p})^{2/(9p)}, \quad (9)$$

where $p = 0.0873$, $m \equiv M(\Gamma h)^3/(\Omega_{m,0}h^2)/10^{12}$. Γ is the shape parameter and is given as

$$\Gamma = \Omega_{m,0}h(T_0/2.7\text{K})^{-2} \exp[-\Omega_B(1 + \sqrt{2h}\Omega_{m,0}^{-1})], \quad (10)$$

where T_0 and Ω_B are the temperature of the cosmic microwave background and the baryon density, which are assumed to be 2.726 K (Mather et al. 1994) and $\Omega_B = 0.0193h^{-2}$ (Burles & Tytler 1998), respectively.

The mass function given above is converted to the XTF by means of a mass-temperature relation. We assume that the ICM in a cluster is described by an isothermal β model (e.g. Forman & Jones 1982), in which the density profile is given as $n_{gas} = n_{gas,0}[1 + (R/R_c)^2]^{-3\beta/2}$, and that hydrostatic equilibrium is achieved. The virial mass is defined as

$$M_v \equiv \frac{4}{3}\pi R_v^3 \rho_0(1 + z)^3\Delta = \frac{3\beta kTR_v}{\mu m_p G}\frac{(R_v/R_c)^2}{1 + (R_v/R_c)^2}, \quad (11)$$

where T is the temperature of ICM, R_v is the virial radius, R_c is the core radius, μ is the mean molecular weight of the ICM (set to 0.6), m_p is the proton mass, G is the gravitational constant, and Δ is the ratio between a cluster mean density and the mean density of the universe at the cluster-formation redshift z. For Δ we use the formula

given in Kitayama & Suto (1996). Since $R_v/R_c >> 1$, the virial mass is approximately given as,

$$M_v = \frac{9}{2}(\pi\rho_0\Delta)^{-1/2}\left(\frac{\beta}{\mu m_p G}\right)^{3/2}\left(\frac{kT}{1 + z}\right)^{3/2} . \quad (12)$$

Note that when $\beta/\beta_{\text{spec}} = 2/3$, ($\beta_{\text{spec}} = \frac{\mu m_p \sigma^2}{kT}$), this equation becomes identical to that derived from a modified singular isothermal sphere by Bryan & Norman (1998). Although an additional modification to the $M - T$ relation is often applied by multiplying a factor accounting for departures from virial equilibrium (e.g. Henry 2000), we did not introduce this factor here. The observed values of β are distributed in a relatively narrow range around $\sim 2/3$ and may show a weakly positive correlation with temperatures (Arnaud & Evrard 1999; Vikhlinin et al. 1999; Horner et al. 1999). Vikhlinin et al. measured β values systematically with *ROSAT* PSPC data excluding a central region inside 30% of the virial radius and found a correlation of β with X-ray temperature, which can be fitted with the linear function $\beta = 0.017\,T(\text{keV}) + 0.621$ (Henry 2000). We employ this relation and substitute it into Eq. 12. The effect of using different $M - T$ relations will be studied in Sect. 5.

We further assume that a cluster collapsed just before it is observed. This recent formation approximation, which has been extensively applied in previous conventional modelings, is relaxed in the Formation-Epoch model described in the next section. Combining all the formulae given above, the model XTF at a given redshift is given by

$$\phi_{ps}(T, z)\,dT = n_{ps}(M_v(T, z), z)\,\frac{dM_v}{dT}(T, z)\,dT . \quad (13)$$

Hereafter we refer to this model XTF as the PS model.

4.2. Formation-Epoch model

In the model XTF given in the previous section, the formation redshift, z_f, of an observed cluster is assumed to be the same as the observed redshift (i.e. recent formation approximation). However, this assumption is not reasonable in particular in a low density universe. Kitayama & Suto (1996) constructed a model XTF taking into account the distribution of the dark-matter-halo formation epoch as well as the evolution of temperature (hereafter FE model). They showed that the XTF predicted by the FE model can be significantly different from the PS model described in Sect. 4.1, in particular when the temperature evolves after the collapse.

The FE model is given as,

$$\phi_{FE}(T_{obs}, z)dT_{obs} = \int_z^\infty dz_f \left[2\frac{\partial p}{\partial z_f}(z_f, 2M_v(T, z_f), z)\right.$$

$$\left. n_{ps}(2M_v(T, z_f), z)\frac{1}{\kappa(z_f, z)}\frac{dM_v}{dT}(T, z_f)\right]dT_{obs} , \quad (14)$$

where n_{ps} and M_v are given in Eqs. 8 and 12, respectively, and $\partial p/\partial z_f$ given by Lacey & Cole (1993) is a differential

distribution function of halo formation epochs of a cluster that has a mass of $2M_{\rm v}$ at the observed redshift z. At the collapse redshift $z_{\rm f}$, the cluster is assumed to be formed with a mass of $M_{\rm v}$, increasing in mass after its formation. $\kappa(z_{\rm f}, z) = \left(\frac{1+z_{\rm f}}{1+z}\right)^s$ gives the evolution in temperature via $T_{\rm obs}(z_{\rm f}, z) = \kappa(z_{\rm f}, z)T(z_{\rm f})$, where $T(z_{\rm f})$ is the virial temperature at the collapse redshift $z_{\rm f}$, while $T_{\rm obs}(z_{\rm f}, z)$ is the observed temperature at the redshift z. $s = 0$ corresponds to no temperature evolution, while $s > 0$ and $s < 0$ indicate positive and negative temperature evolution after the collapse, respectively.

4.3. Fitting method

Instead of fitting the model XTF to the XTF derived in Sect. 3, we use the predicted XTF and the $L - T$ relation to calculate the expected luminosity and temperature distribution for the given survey selection function which is given in a form of $V_{\rm max}$, and perform a fit to the observed luminosity-temperature distribution of the 61 clusters selected in Sect. 2.4. In this analysis, the intrinsic luminosity distribution for a given temperature, which in other words is the conditional luminosity function at a given temperature, is assumed to follow a Gaussian function in logarithmic scale with a constant standard deviation and a mean luminosity given by a power-law function of the temperature. This assumption can be justified by observational results as shown in Sect. 3.1. In order to simplify a model calculation, we assume that the XTF does not change within the search volume of our flux limit and use a model XTF at the median redshift of our cluster sample at z=0.046 as a representative value. Systematic errors on the final results caused from this assumption are found to be negligibly small compared with statistical errors. Incorporated by another Gaussian that represents temperature measurement errors, the expected cluster number density in a unit logarithmic temperature and a unit logarithmic luminosity is given as

$$N(L, T)\, d\log L\, d\log T =$$
$$\int_{-\infty}^{\infty} dT' \left[\frac{\phi(T', z = 0.046)}{(h = 0.71)^3} v_{\rm max}(L, T') \right.$$
$$\frac{1}{\sqrt{2\pi\sigma_{\log L}^2}} \exp\left\{ -\frac{(\log AT^\alpha - \log L)^2}{2\sigma_{\log L}^2} \right\}$$
$$\left. \frac{1}{\sqrt{2\pi\sigma_{\rm T}^2}} \exp\left\{ -\frac{(T' - T)^2}{2\sigma_{\rm T}^2} \right\} \frac{dT}{d\log T} \right] d\log L\, d\log T, \quad (15)$$

where ϕ is calculated for $h = 0.71$ and normalized with the h^{-3} factor to a case of the $h = 1$ universe. $v_{\rm max}(L, T)$ is a maximum comoving volume calculated for $h = 1$, in which a cluster having a temperature of T and a luminosity of L could have been detected under our sample selection criteria, for which the calculation method is given by Eq. A.9. The temperature measurement errors are $\sigma_{\rm T} = 0.051 + 0.0014\, T^{2.585}$ from our *ASCA* results. Free parameters to a fit are; σ_8 and $\Omega_{\rm m,0}$ specifying ϕ;

A and α specifying the power-law function of the $L - T$ relation that gives the mean of the luminosity; and $\sigma_{\log L}$ that is the constant standard deviation of the luminosity from the $L - T$ relation in logarithmic scale. Although $v_{\rm max}$ varies with the assumed model universe, i.e. with the values of $\Omega_{\rm m,0}$ as well as σ_8 which are the fitting parameters, we used a specific $v_{\rm max}$ value calculated with $(\Omega_{\rm m,0}, \Omega_{\Lambda,0}) = (0.2, 0)$, or $(0.2, 0.8)$, in the case of an open or flat universe, respectively. Since all the clusters in our sample are nearby, $v_{\rm max}$ is virtually constant for different $\Omega_{\rm m,0}$ values, using the fixed $v_{\rm max}$ does not introduce any considerable systematic error on the final constraints on $\Omega_{\rm m,0}$ and $\Omega_{\Lambda,0}$. The model cluster distribution was then fitted to the observed temperature and luminosity distribution. Assuming a Poisson distribution of cluster number counts at a given luminosity and temperature, we defined a logarithmic likelihood function as

$$\ln \mathcal{L} = \sum_{\rm i} \ln N(T_{\rm i}, L_{\rm i}) - \int N(T, L)\, d\log L\, d\log T\ , \quad (16)$$

where i denotes each sample cluster and the integration is performed over the $\log L (\rm ergs\, s^{-1})$ range from 41.5 to 45.5 and the $\log T (\rm keV)$ range from 0.14 to 1.05 (corresponding to T = 1.4 – 11.2 keV). By maximizing the likelihood function, we derived the best-fit model XTF as well as the $L - T$ relation.

There are two reasons for setting the low temperature cut-off at 1.4 keV. First, as discussed in Sect. 2.3, the $L-T$ relation breaks down for elliptical galaxies which have a lower gas mass fraction, and actually gets steeper below ~ 1 keV as shown by e.g. Xue & Wu (2000). Thus the simple power-law modeling for the $L - T$ relation is not appropriate for the whole temperature range. The second reason is based on the more essential problem concerned with the comparison between the theoretical XTFs and the observation. The systems at the low temperature end are mostly single elliptical galaxies and some of them may not be isolated but surrounded by larger scale dark matter halos. As has been shown by e.g. Matsushita (1998), X-ray brightness profiles of elliptical galaxies have large variety suggesting a significant variation in total mass for a given temperature, i.e. a considerable scatter in the $M - T$ relation would be expected. Therefore, a cluster abundance at the low temperature end probably does not directly correspond to an abundance of dark matter halos at a certain mass scale.

4.4. Results

We first present the results from the PS model fitting. The best-fit values and errors of the fitting parameters are summarized in Table 3. The best-fit distribution function in the $\log L - \log T$ space in the flat universe case is illustrated in Fig. 7. The corresponding model XTF is also illustrated in Fig. 4. The constraint in $\Omega_{\rm m,0} - \sigma_8$ space is shown in Fig. 8 for each open and flat universe case. The contours represent the 90% confidence range for two parameters of interest, and the constraint is notably tight.

In order to demonstrate an improvement on the constraint by the widest temperature range and the largest sample ever achieved, we also performed the fitting with the PS model only using 51 sample clusters above 3 keV. As shown in Fig. 8, the improvement is significant, in particular, for $\Omega_{m,0}$. Since $\Omega_{m,0}$ is tightly related to the overall shape of the mass variance, i.e. the power spectrum, a larger mass range to measure the mass fluctuation amplitude is essential.

The "true" $L - T$ relation employed in Sect. 2.3 and Sect. 3.1 was estimated by this fitting. Fixing the α value as obtained in Sect. 2.3, to 2.47 and 2.50 for the open and flat universe case, respectively, we performed the PS model fitting and derived $\log A=42.15$, $\sigma = 0.24$ for the open universe case, and $\log A=42.14$, $\sigma = 0.24$ for the flat universe case, which are given in Eqs. 3 and 4 and are applied in Eq. 6.

The FE model gives somewhat different results. In addition to $\Omega_{m,0}$ and σ_8, the FE model introduces another parameter, s, that models a temperature evolution, which can be a free parameter in a fit. However, following Kitayama & Suto (1996), in the following analysis, we rather fixed s at $s = 0$ and $s = 1$ such that they represent no evolution and a maximum possible positive evolution of the temperature, respectively. Since there is no observational evidence for the evolution of the temperature, e.g. no redshift dependency in the $L - T$ relation is found (Mushotzky & Scharf 1997; Donahue et al. 1999; Della Ceca et al. 2000), the no evolution model may be more plausible. However, the effect of the temperature evolution is still interesting to study here. The fitting results are summarized in Table 3, and the constraints on $\Omega_{m,0}$ and σ_8 are illustrated in Fig. 9. The FE model in the no temperature evolution case ($s = 0$) shows similar results with those of the PS model, since the XTF predicted by the $s = 0$ FE model is very close to that of the PS model (see Fig.8 in Kitayama & Suto 1996). On the other hand, in the maximum temperature evolution cases ($s = 1$), the FE model gives significantly smaller σ_8 values than those with the PS model.

5. Discussion

5.1. Uncertainty in the $M - T$ relation

The $M - T$ relation used in our analysis may be subject to uncertainties introducing a significant systematic error in the final results on the cosmological parameters. Theoretical arguments yield a scaling law, that is $M \propto T^{3/2}$ (e.g. Kaiser 1986). A number of numerical simulations support this scaling law, but different normalizations are derived from different simulations. Henry (2000) summarized such differences in the normalization of the $M-T$ relation derived from different hydrodynamical simulations. A cluster mass may vary from 62% to 119% of the mean value.

The $M - T$ relations derived observationally from X-ray mass measurements give somewhat different results.
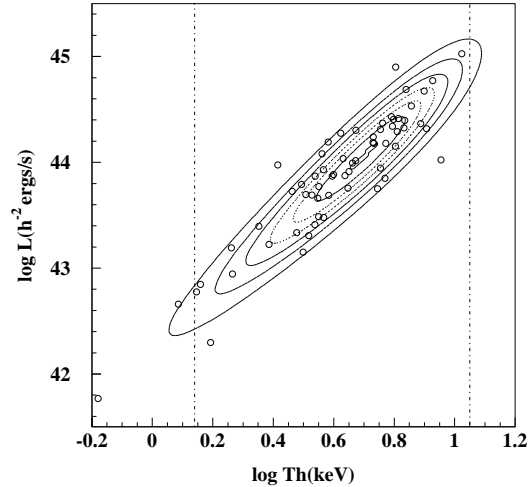

Fig. 7. The best-fit model function in the luminosity-temperature space for the case of the flat universe is shown with contours. The 63 clusters from the flux-limited complete sample are overlayed with open circles. The vertical dotted lines indicate the temperature range used for the fitting. Therefore, 61 clusters are used to make constraints.

Horner et al. (1999) derived an $M - T$ relation which has a similar exponent as the scaling law but a lower normalization than the numerical simulations. On the other hand, Nevalainen et al. (2000) and Finoguenov et al. (2001) obtained steeper relations of $T^{1.79}$ and $T^{1.78}$, respectively, and lower normalizations.

In order to investigate the effects of the different $M-T$ relations, we repeated the fitting performed in Sect. 4 with the PS model for the flat universe case. The six $M - T$ relations we have examined are summarized in Table 4. Each $M - T$ relation can be expressed with Eq. 12, replacing the β value with the formula given in Table 4. In Fig. 10, the best-fit parameters derived with the different $M - T$ relations are compared with the result presented in Sect. 4.4. The effect of using different $M - T$ relations is significant and the systematic errors introduced are comparable to, or even larger than, the current statistical errors. As seen in Fig. 10, a change in the index of the $M - T$ relation moves the best-fit point along the elongation direction of the confidence contour, while an amplitude change moves the best-fit point along the perpendicular direction. Taking into account these systematics from the different $M-T$ relations, the constraints on $\Omega_{m,0}$ and σ_8 are revised and summarized in Table 5.

With the FE model, where the recent formation approximation is not valid, it is not appropriate to use the empirical $M - T$ relation obtained based on the observations of nearby clusters. This is because the current $M-T$ relation should be a result of accumulation of different $M - T$ relations from different formation redshifts which
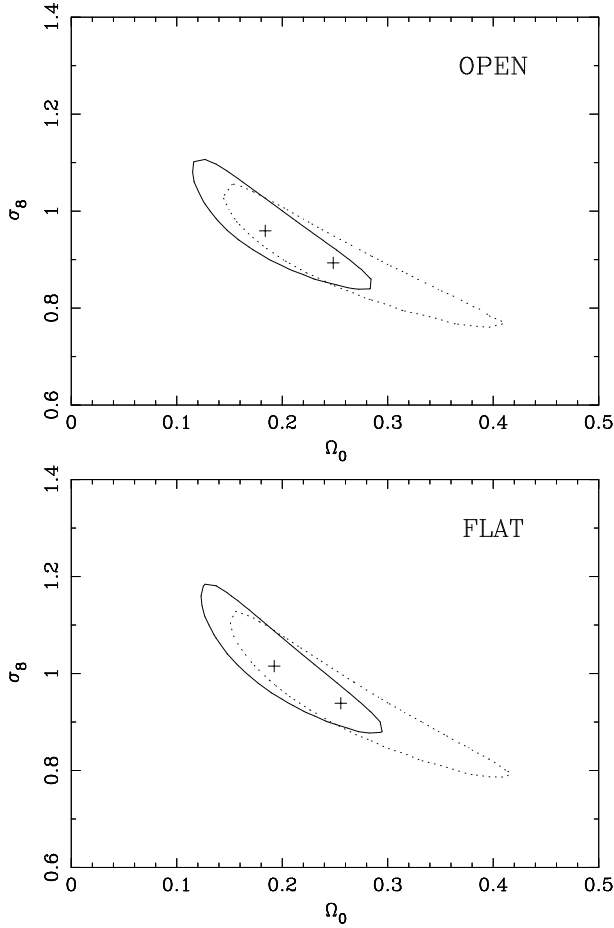
Fig. 8. Constraints on $\Omega_{m,0}$ and σ_8 with the PS model in case of the open (upper panel) and flat (lower panel) universe. Bold contours are results including all sample clusters hotter than 1.4 keV, while dotted contours are derived when only clusters hotter than 3.0 keV are used.

Table 4. M-T relations

Source	β
Hydrodynamic simulation (mean)	$\frac{2}{3} \times 1.21$
Hydrodynamic simulation (maximum)	$\frac{2}{3} \times 1.36$
Hydrodynamic simulation (minimum)	$\frac{2}{3} \times 0.88$
Horner et al.	$0.496\ T^{-0.133}$
Nevalainen et al.	$0.437\ T^{0.193}$
Finoguenov et al.	$0.415\ T^{0.187}$

depend on the cluster masses. Therefore, the $M - T$ relations obtained from the Hydrodynamic simulations may be more appropriately applied with the FE model.

5.2. Comparison with other measurements

We compared our constraints on the cosmological parameters with previous works. Bahcall (2000) summarized the cluster constraints on $\Omega_{m,0}$ and σ_8 as 0.2 ± 0.1 and 1.2 ± 0.2 (68% confidence level), respectively. These values are consistent with our results.

Fig. 9. Constraints on $\Omega_{m,0}$ and σ_8 in case of the open (upper panel) and flat (lower panel) universe. Thin closed contours show results with the PS model. Bold dotted and solid closed contours are derived with the $s = 1$ and $s = 0$ FE models, with and without a temperature evolution effect, respectively. The line shows the constraints from the *COBE* normalization by Bunn & While (1997) for $h = 0.71$.

Table 5. Results with different M-T relations. The parameter ranges correspond to 90% statistical error for one parameter of interest plus systematic errors with different $M - T$ relations applied.

Model XTF	$\Omega_{m,0}$	σ_8
PS(Open)	$0.09 - 0.37$	$0.55 - 1.13$
FE(Open,s=0)	$0.07 - 0.32$	$0.61 - 1.15$
FE(Open,s=1)	$0.03 - 0.23$	$0.52 - 0.80$
PS(Flat)	$0.10 - 0.38$	$0.57 - 1.19$
FE(Flat,s=0)	$0.10 - 0.35$	$0.65 - 1.33$
FE(Flat,s=1)	$0.06 - 0.18$	$0.66 - 0.97$

The power spectrum of matter distribution in the present universe has been measured from the spatial distribution of galaxies and galaxy clusters, and found to be generally well reproduced by the CDM power spectrum (Peacock & West 1992; Einasto et al. 1993; Jing &

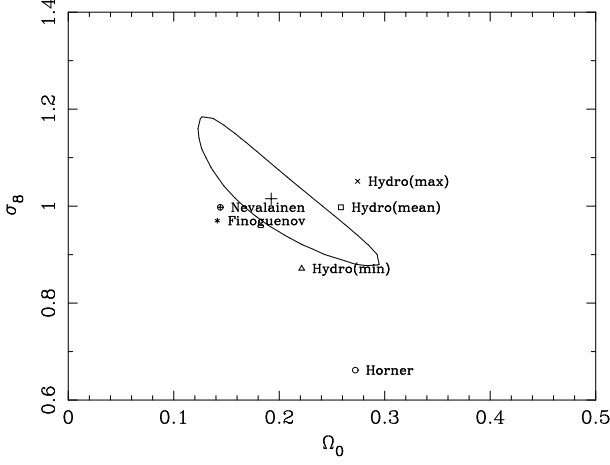**Fig. 10.** The best-fit values of $\Omega_{m,0}$ and σ_8 derived with the PS model in the case of the flat universe, for which different $M-T$ relations are applied. A 90% confidence contour derived in Sect. 4 is also overlayed.

Valadarnini 1993; Einasto et al. 1997; Retzlaff et al. 1998; Tadros et al. 1998; Miller & Batuski 2001). An important feature of the power spectra is a turnover, where the scale is closely linked to the horizon scale at matter-radiation equality. Most recently Schuecker et al. (2001), using a sample of 452 X-ray selected clusters of galaxies, determined the location of the maximum of the power spectrum in the range of $0.022 < k_{max} < 0.030 \; h \; \mathrm{Mpc}^{-1}$. According to the CDM power spectrum, k_{max} is well approximated by

$$k_{max} = 0.114 \; \Gamma \; h \; \mathrm{Mpc}^{-1} \; , \tag{17}$$

where Γ, given in Eq. 10, is a function of $\Omega_{m,0}$. Therefore one finds $0.33 < \Omega_{m,0} < 0.44$. The constraints on $\Omega_{m,0}$ we have derived in Sect. 5.1 with the PS model yield $0.005 < k_{max} < 0.027 \; h \; \mathrm{Mpc}^{-1}$, which overlaps with the result by Schuecker et al. Our results with the FE model give $4 \times 10^{-4} < k_{max} < 0.022 \; h \; \mathrm{Mpc}^{-1}$ in the case of the open universe, and $2 \times 10^{-3} < k_{max} < 0.025 \; h \; \mathrm{Mpc}^{-1}$ in the case of the flat universe, both of which are also consistent with the result by Schuecker et al.

A measurement of the matter density fluctuation at the largest spatial scale was performed using the *COBE* DMR experiment (e.g. Bennett et al. 1996). Bunn & White (1997), using the CDM power spectrum model, extrapolated the *COBE* results to cluster scales and gave constraints in $\Omega_{m,0}$-σ_8 space, which are shown in Fig. 9. In the case of the open universe, our results with any of the model XTFs do not overlap the *COBE* constraints, even if the effects of the uncertainty in the $M-T$ relation are taken into account. On the other hand, in the case of the flat universe, our results with the effects of the uncertainty in the $M-T$ relation, are consistent with the *COBE* constraints regardless of the choice of the model XTF.

6. Summary and Conclusions

The most important result concerning the XTF derived here is that it covers a large enough range of temperatures to reveal the shape of the function beyond a simple power law representation. As expected from theoretical considerations, there should be a very sharp cut-off at the high mass end and the function should turn into a shallower slope at the low mass end as shown by our observations. We have demonstrated that these constraints on the actual slope of the XTF allow us to derive independent constraints on the two parameters which are most important in cosmic structure formation models: $\Omega_{m,0}$ and σ_8. Leaving out only 16% of the sample clusters from the low temperature end almost doubles the uncertainty for these independent constraints. Therefore, while these independent constraints are an important achievement of the present work on one hand, this demonstration also shows that these constraints are sensitive to any systematic error introduced into the XTF.

For this reason we have studied the stability of our results to variations introduced to the observed data and also variations of the theoretical modeling. We have fully incorporated the measurement errors in fluxes and temperatures of the sample clusters. With the typical errors of 5% for the flux and 6-10% for the temperature, the biases were found to be relatively small and not to cause a drastic change on the final results in our analysis. On the other hand, we have shown that there are considerable variations and uncertainties in the theoretical modeling of the XTF, which introduce significant systematic errors in the final constraints on $\Omega_{m,0}$ and σ_8. Various $M-T$ relations that are employed to model the XTF have resulted in considerably different values of $\Omega_{m,0}$ and σ_8. Another source of variation in the theoretical modeling that we have studied is a recent formation approximation which is employed with the Press-Schechter formalism to build the PS model here. Using the FE model, in which the distribution of cluster formation redshifts and the evolution of the mass as well as temperature of a cluster after the collapse are analytically formulated, we have shown that a considerable difference could be introduced in the derived cosmological parameters, in particular in σ_8. This further motivates us to establish a more sophisticated model to the XTF incorporating new X-ray observations of the high redshift clusters with Chandra and XMM-Newton.

Finally, taking into account all the uncertainties, we put our general constraints on $\Omega_{m,0}$ and σ_8 as $\Omega_{m,0}$=0.03–0.37, σ_8=0.52–1.15 in an open universe and $\Omega_{m,0}$=0.06–0.38, σ_8=0.57–1.33 in a flat universe, respectively. From the comparison with the *COBE* constraints, a flat universe is more preferable than an open universe.

Appendix A: Calculation of V_{max}

Here we present our method, used in Sect. 3, to evaluate the X-ray temperature function in more detail. A flux limited sample has been extensively used for constructing

the X-ray luminosity function (XLF) by many authors (e.g. Piccinotti et al. 1982; Edge et al. 1990; Gioia et al. 1990; Henry et al. 1992; Ebeling et al. 1997; Rosati et al. 1998; de Grandi et al. 1999; Ledlow et al. 1999). Here we present the first description of how to construct this function in the presence of measurement uncertainties, correlation scatter and selection biases. For a sample with a finite number of objects, the differential XLF, i.e. the number density of clusters having the rest frame luminosity in a range of $L - \frac{\Delta L}{2}$ to $L + \frac{\Delta L}{2}$ defined in a comoving space, can be evaluated as

$$\phi(L)\Delta L = \sum_{L-\frac{\Delta L}{2} \leq L_i < L+\frac{\Delta L}{2}} \frac{1}{v_{\max}(L_i, T_i)} \ , \qquad (A.1)$$

where i denotes individual clusters in the luminosity range of a bin. $v_{\max}(L, T)$ is a maximum search volume measured in comoving space where a cluster having the rest frame luminosity of L and the temperature of T could have been detected under the flux limited condition. Introducing $z_{\max}$, the maximum redshift at which such a cluster could have been detected, and V_{com}, a total volume in the comoving coordinate from us to a given redshift, we can derive $v_{\max}(L, T)$ as

$$v_{\max}(L, T) = \frac{\Omega}{4\pi} V_{\text{com}}(z_{\max}) \ , \qquad (A.2)$$

where Ω is the total sky coverage in steradians, and V_{com} is, in the case of a flat universe, simply given by

$$V_{\text{com}}(z) = \frac{4\pi}{3} \left\{ \frac{D_l(z)}{1+z} \right\}^3 \ , \qquad (A.3)$$

where D_l is a luminosity distance, while, in the case of an open universe, it is given with a more complicated form (see e.g. Sandage 1988). $z_{\max}$ is given by solving the following equation

$$D_l(z_{\max})^2 = \frac{L_{\text{obs}}(L, T, z_{\max})}{4\pi f_{\text{obs,lim}}} \ , \qquad (A.4)$$

where $f_{\text{obs,lim}}$ is the flux limit defined in a certain energy range in the observed frame, and L_{obs} is the same observed-frame luminosity that is expected if the cluster is located at $z_{\max}$. In order to solve this equation with the K-correction, the spectral energy distribution, i.e. the temperature, T, is required, although the dependency of $z_{\max}$ on T is generally weak.

Using $v_{\max}(L, T)$, the differential XTF can be given as

$$\phi(T)\Delta T = \sum_{T-\frac{\Delta T}{2} \leq T_i < T+\frac{\Delta T}{2}} \frac{1}{v_{\max}(L_i, T_i)} \ . \qquad (A.5)$$

This estimator is used in e.g. Henry (2000). However, since there is a distribution of luminosities for a given temperature, this method introduces a scatter in a derived XTF, unless there are large numbers of clusters in each temperature bin. If the distribution of the luminosity for a given temperature is known, we can obtain an average search volume by summing $v_{\max}(L, T)$ in a whole range of luminosities weighted with the probability. Assuming that

luminosities for a given temperature are distributed like a Gaussian with a mean given by the power-law function, $L = AT^\alpha$, and with a constant standard deviation, in logarithmic scale, we can obtain the average search volume at a given temperature as

$$V_{\max}(T) =$$
$$\int_{-\infty}^{\infty} \frac{v_{\max}(L, T)}{\sqrt{2\pi\sigma_{\log L}^2}} \exp\left[-\frac{(\log AT^\alpha - \log L)^2}{2\sigma_{\log L}^2} \right] d\log L. \ (A.6)$$

We can then evaluate the temperature function as

$$\phi(T)\Delta T = \sum_{T-\frac{\Delta T}{2} \leq T_i < T+\frac{\Delta T}{2}} \frac{1}{V_{\max}(T_i)} \ . \qquad (A.7)$$

Performing Monte-Carlo simulations, we confirmed that both estimators, the $1/v_{\max}(L, T)$ method and $1/V_{\max}(T)$ method are consistent and unbiased, that is they reproduce the temperature function fed to the simulations in the limit of an infinite number of simulated clusters, and the mean value of the temperature functions obtained from a number of independent measurements with a finite number of clusters is also equal to the true value in the limit of an infinite number of measurements. However, the $1/V_{\max}(T)$ method gives smaller variance in a measurement of the temperature function and therefore it is more efficient than the $1/v_{\max}(L, T)$ method. This is well demonstrated in Fig. 4.

When we apply this analysis method to our cluster sample, we further consider the following two points: Our first concern is that the flux measurement may have a redshift bias such that for clusters with the same true luminosity, different luminosities are derived for different redshifts. In order to study this effect we produced a sample of cluster images at various redshifts as observed by the *ROSAT* PSPC and determined their fluxes with the growth curve analysis method (Böhringer et al. 2000) as performed for the actual observed data of the present sample by Reiprich & Böhringer (2002). The simulations show that the resulting luminosities are kept constant regardless of the redshift — at least in a range that we are considering here, i.e. $z < 0.2$, despite the overall signal to noise ratio worsening with a dimming of the surface brightness that follows $(1 + z)^{-4}$.

Secondly, the effect from the measurement errors on X-ray fluxes is considered. If there are considerable measurement errors in the flux measurements, a cluster that should be in the flux-limited sample could be found to be fainter than the flux limit and to be missed from the sample, and vice-versa. If the measured flux distribution is assumed to be following a Gaussian function with the sigma value of σ_f, the probability that a cluster of the luminosity L at the redshift of z is found to be brighter than the flux limit $f_{\lim}$ is given as

$$W(L, z, f_{\lim}) = \int_{f_{\lim}}^{\infty} \frac{1}{\sqrt{2\pi\sigma_f^2}} \exp\left[-\frac{(f - f_0)^2}{2\sigma_f^2} \right] df \ , \ (A.8)$$

where $f_0 = L/4\pi D_l(z)^2$. Therefore, Eq. A.2 should be modified as

$$v_{\max}(L, T) = \frac{\Omega}{4\pi} \int_0^\infty \frac{dV_{\rm com}}{dz} W(L, D_l, f_{\lim}) dz \ . \qquad {\rm (A.9)}$$

Setting $\sigma_{\rm f}$ to 10^{-12} ergs s^{-1} cm^{-2}, a typical flux measurement error around the flux limit, this modification brings a 2% and 0.5% increase to $v_{\max}(L, T)$ at 1 and 10 keV, respectively, compared with the simple estimate with Eq. A.2.

Although the correction is still insignificant with respect to the Poisson error that each temperature bin would have, we use the Eq. A.9 in the derivation of the XTF in Sect. 3. Our sample selection criteria specify several parameters in Eq. A.5, A.6, A.8 and A.9 as $\Omega = 8.139$ str, $f_{\rm obs,lim} = 1.99 \times 10^{-11}$ ergs s^{-1} cm^{-2} in 0.1-2.4 keV band in the observed frame, and then $L_{\rm obs}$ should be the 0.1-2.4 keV band luminosity in the observed frame, which corresponds to a cluster rest frame luminosity in the energy range from $(1 + z_{\max})$ 0.1 to $(1 + z_{\max})$ 2.4 keV. Also, from the $L - T$ relation studied in Sect. 2.3 and Sect. 4, we estimated the following parameters as $\log A = 42.15$, $\alpha = 2.47$, and $\sigma_{\log L} = 0.24$ for an open universe case, and $\log A = 42.14$, $\alpha = 2.50$, and $\sigma_{\log L} = 0.24$ for a flat universe case. The XTF thus derived is shown in Fig. 4.

Finally, we should note that $T_{\rm i}$ in Eq. A.5 is the measured cluster temperature rather than the "true" temperature. The derived XTF should have been smeared due to the temperature measurement error, which brings another systematic error into the resulting XTF. In order to investigate the possible systematic errors due to the temperature measurement errors and to confirm our analysis method, we performed a Monte-Carlo simulation. With an adopted XTF of $\phi(T) \propto T^{-5}$, a number of cluster observations are simulated taking into account the scatter in the $L - T$ relation as well as the flux and temperature measurement errors, and the XTF was constructed as performed with the real data using Eqs. A.5, A.6, A.8 and A.9. The input XTF and the rederived XTF from the simulations show complete agreement except a minor systematic increase — at most 2% at 10 keV, which is due to the temperature measurement error for very hot clusters. These systematics (Eddington bias; Eddington 1944) remain in the XTF derived in Sect. 3 (Fig. 4), while, for the model fitting in Sect. 4, the temperature measurement error is taken into account (Eq. 15).

References

Akritas, M. G. & Bershady, M. A. 1996, ApJ, 470, 706

Allen, S. W., Fabian, A. C., Johnstone, R. M., Arnaud, K. A., & Nulsen, P. E. J. 2001, MNRAS, 322, 589

Allen, S. W. 2000, MNRAS, 315, 269

Arnaud, K.A., 1996, Astronomical Data Analysis Software and Systems V, eds. Jacoby G. & Barnes J., ASP Conf. Series, volume 101, 17

Arnaud, M., & Evrard, A. E. 1999, MNRAS, 305, 631

Böhringer 1999, private communication

Böhringer, H., Voges, W., Huchra, J. P., et al. 2000, ApJS, 129, 435

Böhringer, H., Schuecker, P., Guzzo, L. 2001, A&A, 369, 826

Bahcall, N. A. & Cen, R. 1993, ApJ, 407, L49

Bahcall, N. A. 2000, Physics Reports, 333-334, 233

Bennett, C. L., Banday, A. J., Gorski, K. M., et al. 1996, ApJ, 464, L1

Beuing, J., Döbereiner, S., Böhringer, H. & Bender, R. 1999, MNRAS, 302, 209

Biviano, A., Girardi, M., Giuricin, G., Mardirossian, F., & Mezzetti, M. 1993, ApJ, 411, L13

Blanchard, A., Sadat., R., Bartlett., J. G., & Le Dour, M. 2000, A&A, 362, 809

Briel, U. G. & Henry, J. P. 1994, Nature, 372, 439

Bryan, G. L. & Norman, M. L. 1998, ApJ, 495, 80

Bunn, E. F. & White, M. 1997, ApJ, 480, 6

Burles, S. & Tytler, D. 1998, ApJ, 499, 699

de Bernardis, P., Ade, P. A. R., Bock, J. J., et al. 2000, Nature, 404, 955

de Grandi, S., Guzzo, L., Böhringer, H., et al. 1999, ApJ, 513, L17

de Grandi, S., Böhringer, H., Guzzo, L., et al. 1999, ApJ, 514, 148

David, L. P., Slyz, A., Jones, C., et al. 1993, ApJ, 412, 479

Della Ceca, R., Scaramella, R., Gioia, I. M., et al. 2000, A&A, 353, 498

Donahue, M., Voit, G. M., Scharf, C. A., et al. 1999, ApJ, 527, 525

Ebeling, H., Voges, W., Böhringer, H., et al. 1996, MNRAS, 281, 799

Ebeling, H., Edge, A. C., Fabian, A. C., et al. 1997, ApJ, 479, L101

Ebeling, H., Edge, A. C., Böhringer, H., et al. 1998, MNRAS, 301, 881

Eddington, A. S. 1940, MNRAS, 100, 354

Edge, A. C., Stewart, G. C., Fabian, A. C., & Arnaud, K. A. 1990, MNRAS, 245, 559

Edge, A. C. & Stewart, G. C. 1991, MNRAS, 252, 414

Einasto, J., Gramann, M., Saar, E. & Targo, E. 1993, MNRAS, 260, 705

Einasto, J, Einasto, M., Gottlöber, S., et al. 1997, Nature, 385, 139

Eke, V. R., Cole, S., Freml, C. S., & Henry, J. P. 1998, MNRAS, 298, 1145

Eke, V. R., Cole, S., & Frenk, C. S. 1996, MNRAS, 282, 263

Evrard, A. E. 1997, MNRAS, 292, 289

Fabian, A. C. 1994, ARA&A, 32, 277

Fabian, A. C., Arnaud, K. A., Bautz, M. W., Tawara, Y. 1994, ApJ, 436, L63

Finoguenov, A., Reiprich, T. H. & Böhringer, H. 2001, A&A, 368, 749

Forman, W. & Jones, C. 1982, ARA&A

Fukazawa, Y., et al. 1994, PASJ, 46, L55

Fukazawa, Y. 1997, PhD thesis, the University of Tokyo

Fukazawa, Y., Makishima, K., Tamura, T., et al. 1998, PASJ, 50, 187

Fukazawa, Y., Makishima, K., Tamura, T., et al. 2000, MNRAS, 313, 21

Gioia, I. M., Henry, J. P., Maccacaro, T., et al. 1990, ApJ, 356, L35

Girardi, M., Borgani, S., Giuricin, G., Mardirossian, F., & Mezzetti, M. 1998, ApJ, 506, 45

Henry, J. P., Gioia, I. M., Maccacaro, T., et al. 1992, ApJ, 386, 408

Henry, J. P. 2000, ApJ, 534, 565

Henry, J. P., & Arnaud, K. A. 1991, ApJ, 372, 410

Horner, D. J., Mushotzky, R. F., & Scharf, C. A. 1999, ApJ, 520, 78

Ikebe, Y., Makishima, K., Ezawa, H., et al. 1997, ApJ, 481, 660

Ikebe, Y., Makishima, K., Fukazawa, Y., et al. 1999, ApJ, 525, 58

Ikebe, Y. 2001, Proceedings of "Tracing Cosmic Evolution with Clusters of Galaxies", Sesto Pusteria, Bolzano, Italy, July 3-6, 2001, astro-ph/0112132

Isobe, T., Feigelson, E. D., Akritas, M. G., & Babu, G. J. 1990, ApJ, 364, 104

Jing, Y. P. & Valadarnini, R. 1993, ApJ, 406, 6

Kaastra, J.S. 1992, An X-Ray Spectral Code for Optically Thin Plasmas (Internal SRON-Leiden Report, updated version 2.0)

Kaastra, J.S., Ferrigno, C., Tamura, T., et al. 2001, A&A, 365, L99

Kaiser, N. 1986, MNRAS, 222, 323

Kitayama, T. & Suto, Y. 1996, ApJ, 469, 480

Lacey, C. G. & Cole, S. 1993, MNRAS, 262, 627

Lahav, O., Edge, A. C., Fabian, A. C. & Putney, A. 1989, MNRAS, 238, 881

Ledlow, M. J., Loken, C., Burns, J. O., Owen, F. N. & Voges, W. 1999, ApJ, 516, L53

Liedahl, D. A., Osterheld, A. L. & Goldstein, W. H. 1995, ApJ, 438, L115

Makishima, K., Ezawa, H., Fukazawa, Y., et al. 2000, PASJ, in press

Markevitch, M. 1998, ApJ, 504, 27

Markevitch, M., Forman, W. R., Sarazin, C. L. & Vikhlinin, A. 1998, ApJ, 503, 77

Mather, J. C., Cheng, E. S., Cottingham, D. A., et al. 1994, ApJ, 420, 439

Matsumoto, H., Koyama, K., Awaki, H., et al. 1996, PASJ, 48, 201

Matsushita, K. 1998, PhD thesis, the University of Tokyo

Mewe, R., Gronenschild, E. H. B. M., & van den Oord, G. H. J. 1985, A&AS, 62, 197

Mewe, R., Lemen, J. R., & van den Oord, G. H. J. 1986, A&AS, 65, 511

Miller, C. J. & Batuski, D. J. 2001, ApJ, 551, 635

Mould, J. R., Huchra, J. P., Freedman, W. L., et al. 2000, ApJ, 529, 786

Mushotzky, R. F. & Scharf, C. A. 1997, ApJ, 482, L13

Nevalainen, J., Markevitch, M. & Forman, W. 2000, ApJ, 536, 73

Ohashi, T., Ebisawa, K., Fukazawa, Y., et al. 1996, PASJ, 48, 157

Oukbir, J. & Blanchard, A. 1997, A&A, 317, 1

Peacock, J. A. & West, M. 1992, MNRAS, 259, 494

Perlmutter, S., Aldering, G., Goldhaber, G., et al. 1999, ApJ, 517, 565

Pen, U. 1998, ApJ, 1998, 498, 60

Peterson, J. R., Paerels, F. B. S., Kaastra, J. S., et al. 2001, A&A, 365, L104

Pfeffermann, E., Briel, U. G., Hippmann, H., et al. 1987, Proceedings of SPIE, 733, 519

Piccinotti, G., Mushotzky, R. F., Boldt, E. A., et al. 1982, ApJ, 253, 485

Pierpaoli, E., Scott, D., & White, M. 2001, MNRAS, 325, 77

Press, W. H. & Schechter, P. 1974, ApJ, 187, 425

Reiprich, T. H., & Böhringer, H., 2002, ApJ, in press, (astro-ph/0111285)

Retzlaff, J., Borgani, S., Gottlöber, S. Klypin, A. & Müller, V. 1998, New Astron., 3, 631

Riess, A. G., Filippenko, A. V., Challis, P., et al. 1998, AJ, 116, 1009

Rosati, P., Della Ceca, R., Norman, C. & Giacconi, R., 1998, ApJ, 492, L21

Sandage, A. 1988, ARA&A, 26, 561

Schuecker, P., Böhringer, H., Guzzo, L., et al. 2001, A&A, 368, 86

Serlemitsos, P. J., Jalota, L., Soong, Y., et al. 1995, PASJ, 47, 105

Tadros, H., Efstathiou, G. & Dalton, G., 1998, MNRAS, 296, 995

Takahashi, T., Markevitch, M., Fukazawa, Y. et al. 1995, *ASCA* Newsl. (NASA/GSFC), 3, 25

Tamura, T., Kaastra, J. S., Peterson, J. R., et al. 2001, A&A, 365, L87

Tanaka, T., Inoue, H., & Holt, S. S. 1994, PASJ, 46, L37

Trümper, J. 1993, Sci, 260, 1769

Viana, P. T. P. & Liddle, A. R. 1996, MNRAS, 281, 323

Vikhlinin, A., Forman, W., & Jones, C. 1999, ApJ, 525, 47

Voges, W., Aschenbach, B., Boller, T., et al. 1999, A&A, 349, 389

White, S. D. M., Efstathiou, G., & Frenk, C. S. 1993, MNRAS, 262, 1023

White, D. A. 2000, MNRAS, 312, 663

Xu, H., Makishima, K., Fukazawa, Y., et al. 1998, ApJ, 500, 738

Xue, Y. & Wu, X. 2000, ApJ, 538, 65

Table 1. Summary of the cluster sample

NAME	redshift	n_{H} $(10^{21}\mathrm{cm}^{-2})$	kT_{h} (keV)	Flux(0.1-2.4keV) $(10^{-11}\mathrm{ergs\ s}^{-1}\ \mathrm{cm}^{-2})$	[†]L_{X} (0.1-2.4keV) $(h^{-2}\ \mathrm{ergs\ s}^{-1}\ \mathrm{cm}^{-2})$ Open	Flat
[*]PERSEUS	0.0183	1.569	$6.42^{+0.06}_{-0.06}$	114.33 ± 1.50	(4.12 ± 0.05)e+44	(4.19 ± 0.05)e+44
[*]OPHIUCHUS	0.0280	2.014	$10.25^{+0.30}_{-0.36}$	36.25 ± 1.16	(3.07 ± 0.10)e+44	(3.14 ± 0.10)e+44
COMA	0.0232	0.089	$8.07^{+0.29}_{-0.27}$	35.13 ± 0.79	(2.04 ± 0.05)e+44	(2.08 ± 0.05)e+44
[*]A3627	0.0163	2.083	$5.62^{+0.12}_{-0.11}$	31.60 ± 1.57	(9.04 ± 0.45)e+43	(9.16 ± 0.45)e+43
A3526	0.0103	0.825	$3.69^{+0.05}_{-0.04}$	26.20 ± 0.95	(2.99 ± 0.11)e+43	(3.02 ± 0.11)e+43
[*]AWM7	0.0172	0.921	$3.70^{+0.08}_{-0.05}$	16.60 ± 0.55	(5.30 ± 0.18)e+43	(5.37 ± 0.18)e+43
[*]A2319	0.0564	0.877	$8.84^{+0.29}_{-0.24}$	12.15 ± 0.21	(4.20 ± 0.07)e+44	(4.39 ± 0.07)e+44
A3571	0.0397	0.393	$6.80^{+0.21}_{-0.18}$	12.00 ± 0.15	(2.05 ± 0.03)e+44	(2.12 ± 0.03)e+44
[*]TRIANGUL	0.0510	1.229	$9.06^{+0.33}_{-0.31}$	11.26 ± 0.13	(3.18 ± 0.04)e+44	(3.31 ± 0.04)e+44
A2199	0.0302	0.084	$4.28^{+0.10}_{-0.10}$	10.73 ± 0.32	(1.06 ± 0.03)e+44	(1.09 ± 0.03)e+44
[*]3C129	0.0223	6.789	$5.57^{+0.16}_{-0.15}$	10.65 ± 0.98	(5.72 ± 0.53)e+43	(5.82 ± 0.54)e+43
A1060	0.0114	0.492	$3.15^{+0.05}_{-0.05}$	10.04 ± 0.54	(1.41 ± 0.07)e+43	(1.42 ± 0.08)e+43
2A0335	0.0349	1.864	$3.64^{+0.09}_{-0.08}$	8.87 ± 0.11	(1.17 ± 0.01)e+44	(1.21 ± 0.01)e+44
A0262	0.0161	0.552	$2.25^{+0.06}_{-0.06}$	8.78 ± 0.55	(2.46 ± 0.15)e+43	(2.49 ± 0.16)e+43
FORNAX	0.0046	0.145	$1.56^{+0.05}_{-0.07}$	8.68 ± 0.66	(1.97 ± 0.15)e+42	(1.98 ± 0.15)e+42
A0496	0.0328	0.568	$4.59^{+0.10}_{-0.10}$	8.20 ± 0.10	(9.56 ± 0.12)e+43	(9.81 ± 0.12)e+43
A0085	0.0556	0.358	$6.51^{+0.16}_{-0.23}$	7.37 ± 0.07	(2.48 ± 0.03)e+44	(2.59 ± 0.03)e+44
A3667	0.0560	0.459	$6.28^{+0.27}_{-0.26}$	7.12 ± 0.08	(2.44 ± 0.03)e+44	(2.54 ± 0.03)e+44
A2029	0.0767	0.307	$7.93^{+0.39}_{-0.36}$	6.88 ± 0.07	(4.43 ± 0.04)e+44	(4.70 ± 0.05)e+44
A3558	0.0480	0.363	$5.37^{+0.17}_{-0.15}$	6.68 ± 0.05	(1.68 ± 0.01)e+44	(1.74 ± 0.01)e+44
[*]S636	0.0116	0.642	$2.06^{+0.07}_{-0.06}$	6.65 ± 0.54	(9.65 ± 0.79)e+42	(9.75 ± 0.79)e+42
A2142	0.0899	0.405	$8.46^{+0.53}_{-0.49}$	6.21 ± 0.09	(5.52 ± 0.08)e+44	(5.90 ± 0.08)e+44
A1795	0.0616	0.120	$6.17^{+0.26}_{-0.25}$	6.21 ± 0.03	(2.58 ± 0.01)e+44	(2.70 ± 0.02)e+44
[*]PKS0745	0.1028	4.349	$6.37^{+0.21}_{-0.20}$	6.13 ± 0.10	(7.18 ± 0.11)e+44	(7.74 ± 0.12)e+44
A2256	0.0601	0.402	$6.83^{+0.23}_{-0.21}$	6.03 ± 0.14	(2.38 ± 0.05)e+44	(2.49 ± 0.06)e+44
A1367	0.0216	0.255	$3.55^{+0.08}_{-0.08}$	5.98 ± 0.07	(3.02 ± 0.04)e+43	(3.07 ± 0.04)e+43
A3266	0.0594	0.148	$7.72^{+0.35}_{-0.28}$	5.77 ± 0.06	(2.22 ± 0.02)e+44	(2.32 ± 0.03)e+44
A4038	0.0283	0.155	$3.22^{+0.10}_{-0.10}$	5.61 ± 0.12	(4.86 ± 0.10)e+43	(4.97 ± 0.10)e+43
A2147	0.0351	0.329	$4.34^{+0.12}_{-0.13}$	5.45 ± 0.29	(7.28 ± 0.39)e+43	(7.49 ± 0.40)e+43
A0401	0.0748	1.019	$7.19^{+0.28}_{-0.24}$	5.26 ± 0.09	(3.23 ± 0.06)e+44	(3.41 ± 0.06)e+44
N5044	0.0090	0.491	$1.22^{+0.04}_{-0.04}$	5.20 ± 0.04	(4.54 ± 0.04)e+42	(4.58 ± 0.04)e+42
A0478	0.0900	1.527	$6.91^{+0.40}_{-0.36}$	5.12 ± 0.05	(4.58 ± 0.04)e+44	(4.89 ± 0.05)e+44
HYDRA-A	0.0538	0.486	$3.82^{+0.20}_{-0.17}$	4.71 ± 0.04	(1.49 ± 0.01)e+44	(1.56 ± 0.01)e+44
A2052	0.0348	0.290	$3.12^{+0.10}_{-0.09}$	4.57 ± 0.08	(6.01 ± 0.10)e+43	(6.18 ± 0.10)e+43
N1550	0.0123	1.159	$1.44^{+0.03}_{-0.02}$	4.24 ± 0.37	(6.93 ± 0.61)e+42	(7.00 ± 0.62)e+42
A2063	0.0354	0.292	$3.56^{+0.16}_{-0.12}$	4.23 ± 0.09	(5.74 ± 0.12)e+43	(5.90 ± 0.12)e+43
A1644	0.0474	0.533	♮$4.70^{+0.90}_{-0.70}$	4.09 ± 0.34	(1.00 ± 0.08)e+44	(1.04 ± 0.09)e+44
A0119	0.0440	0.310	$5.69^{+0.24}_{-0.28}$	4.05 ± 0.06	(8.53 ± 0.13)e+43	(8.82 ± 0.13)e+43
[*]A0644	0.0704	0.514	$6.54^{+0.27}_{-0.26}$	3.97 ± 0.07	(2.16 ± 0.04)e+44	(2.28 ± 0.04)e+44
N4636	0.0037	0.175	$0.66^{+0.03}_{-0.01}$	3.97 ± 0.47	(5.84 ± 0.69)e+41	(5.86 ± 0.69)e+41
A3158	0.0590	0.106	$5.41^{+0.26}_{-0.24}$	3.79 ± 0.09	(1.44 ± 0.04)e+44	(1.51 ± 0.04)e+44
A1736	0.0461	0.536	$3.68^{+0.22}_{-0.17}$	3.54 ± 0.36	(8.21 ± 0.84)e+43	(8.51 ± 0.87)e+43
A0754	0.0528	0.459	$9.00^{+0.35}_{-0.34}$	3.34 ± 0.09	(1.01 ± 0.03)e+44	(1.06 ± 0.03)e+44
A0399	0.0715	1.058	$6.46^{+0.38}_{-0.36}$	3.30 ± 0.29	(1.85 ± 0.16)e+44	(1.95 ± 0.17)e+44
MKW3S	0.0450	0.315	$3.45^{+0.13}_{-0.10}$	3.22 ± 0.05	(7.13 ± 0.12)e+43	(7.38 ± 0.12)e+43
[*]A0539	0.0288	1.206	$3.04^{+0.11}_{-0.10}$	3.12 ± 0.07	(2.80 ± 0.06)e+43	(2.87 ± 0.06)e+43
EXO0422	0.0390	0.640	♮$2.90^{+0.90}_{-0.60}$	3.12 ± 0.32	(5.16 ± 0.52)e+43	(5.32 ± 0.54)e+43
A4059	0.0460	0.110	$3.94^{+0.15}_{-0.15}$	3.10 ± 0.07	(7.16 ± 0.16)e+43	(7.42 ± 0.16)e+43
A3581	0.0214	0.426	$1.83^{+0.04}_{-0.02}$	3.08 ± 0.16	(1.53 ± 0.08)e+43	(1.55 ± 0.08)e+43
A3112	0.0750	0.253	$4.72^{+0.37}_{-0.25}$	3.07 ± 0.06	(1.90 ± 0.03)e+44	(2.01 ± 0.04)e+44
A0576	0.0381	0.569	$3.83^{+0.16}_{-0.15}$	2.99 ± 0.33	(4.73 ± 0.53)e+43	(4.88 ± 0.54)e+43
A3562	0.0499	0.391	$4.47^{+0.23}_{-0.21}$	2.89 ± 0.04	(7.87 ± 0.12)e+43	(8.18 ± 0.13)e+43
A2204	0.1523	0.594	$6.38^{+0.23}_{-0.23}$	2.73 ± 0.07	(7.13 ± 0.19)e+44	(7.92 ± 0.21)e+44
A0400	0.0240	0.938	$2.43^{+0.13}_{-0.12}$	2.64 ± 0.05	(1.65 ± 0.03)e+43	(1.68 ± 0.03)e+43

Table 1. continued

NAME	redshift	n_{H} $(10^{21}\mathrm{cm}^{-2})$	kT_{h} (keV)	Flux(0.1-2.4keV) $(10^{-11}\mathrm{ergs\ s}^{-1}\mathrm{\ cm}^{-2})$	[†]L_{X} (0.1-2.4keV) $(h^{-2}\mathrm{\ ergs\ s}^{-1}\mathrm{\ cm}^{-2})$ Open	Flat
A2065	0.0721	0.284	$5.37^{+0.34}_{-0.30}$	2.55 ± 0.26	$(1.46 \pm 0.15)\mathrm{e}{+}44$	$(1.54 \pm 0.15)\mathrm{e}{+}44$
A1651	0.0860	0.171	$6.22^{+0.45}_{-0.41}$	2.52 ± 0.05	$(2.06 \pm 0.04)\mathrm{e}{+}44$	$(2.19 \pm 0.04)\mathrm{e}{+}44$
A2589	0.0416	0.439	$3.38^{+0.13}_{-0.13}$	2.52 ± 0.05	$(4.75 \pm 0.10)\mathrm{e}{+}43$	$(4.91 \pm 0.11)\mathrm{e}{+}43$
MKW8	0.0270	0.260	$3.29^{+0.23}_{-0.22}$	2.51 ± 0.35	$(1.99 \pm 0.27)\mathrm{e}{+}43$	$(2.03 \pm 0.28)\mathrm{e}{+}43$
A2657	0.0404	0.527	$3.53^{+0.12}_{-0.12}$	2.49 ± 0.04	$(4.44 \pm 0.06)\mathrm{e}{+}43$	$(4.58 \pm 0.07)\mathrm{e}{+}43$
A3376	0.0455	0.501	$4.43^{+0.39}_{-0.38}$	2.44 ± 0.06	$(5.52 \pm 0.13)\mathrm{e}{+}43$	$(5.72 \pm 0.14)\mathrm{e}{+}43$
S1101	0.0580	0.185	$\flat 2.60^{+0.50}_{-0.50}$	2.44 ± 0.04	$(9.05 \pm 0.14)\mathrm{e}{+}43$	$(9.46 \pm 0.14)\mathrm{e}{+}43$
A1650	0.0845	0.154	$5.68^{+0.30}_{-0.27}$	2.43 ± 0.26	$(1.92 \pm 0.21)\mathrm{e}{+}44$	$(2.04 \pm 0.22)\mathrm{e}{+}44$
A2634	0.0312	0.517	$3.45^{+0.16}_{-0.16}$	2.38 ± 0.06	$(2.51 \pm 0.06)\mathrm{e}{+}43$	$(2.58 \pm 0.07)\mathrm{e}{+}43$
A3391	0.0531	0.542	$5.89^{+0.45}_{-0.33}$	2.20 ± 0.07	$(6.78 \pm 0.21)\mathrm{e}{+}43$	$(7.06 \pm 0.22)\mathrm{e}{+}43$
A2597	0.0852	0.250	$4.20^{+0.49}_{-0.41}$	2.20 ± 0.04	$(1.77 \pm 0.04)\mathrm{e}{+}44$	$(1.88 \pm 0.04)\mathrm{e}{+}44$
ZwCl1215	0.0750	0.164	$\flat 6.30^{+2.68}_{-1.88}$ $\sharp 6.36^{+2.94}_{-2.01}$	2.17 ± 0.05	$(1.34 \pm 0.03)\mathrm{e}{+}44$	$(1.42 \pm 0.03)\mathrm{e}{+}44$
A2244	0.0970	0.207	$5.77^{+0.61}_{-0.44}$	2.10 ± 0.07	$(2.19 \pm 0.08)\mathrm{e}{+}44$	$(2.35 \pm 0.08)\mathrm{e}{+}44$
A0133	0.0569	0.160	$3.97^{+0.28}_{-0.27}$	2.06 ± 0.03	$(7.33 \pm 0.10)\mathrm{e}{+}43$	$(7.66 \pm 0.11)\mathrm{e}{+}43$
A2163	0.2010	1.227	$10.55^{+1.01}_{-0.68}$	2.04 ± 0.05	$(9.28 \pm 0.23)\mathrm{e}{+}44$	$(10.59 \pm 0.27)\mathrm{e}{+}44$
A2255	0.0800	0.251	$5.92^{+0.40}_{-0.26}$	2.02 ± 0.04	$(1.42 \pm 0.03)\mathrm{e}{+}44$	$(1.51 \pm 0.03)\mathrm{e}{+}44$
IIIZw54	0.0311	1.668	$\flat 2.98^{+1.27}_{-0.89}$ $\sharp 3.00^{+1.39}_{-0.95}$	2.01 ± 0.25	$(2.11 \pm 0.27)\mathrm{e}{+}43$	$(2.16 \pm 0.27)\mathrm{e}{+}43$
A3395s	0.0498	0.849	$5.55^{+0.89}_{-0.65}$	2.01 ± 0.13	$(5.42 \pm 0.34)\mathrm{e}{+}43$	$(5.63 \pm 0.35)\mathrm{e}{+}43$
N507	0.0165	0.525	$1.40^{+0.04}_{-0.07}$	2.00 ± 0.04	$(5.88 \pm 0.12)\mathrm{e}{+}42$	$(5.96 \pm 0.12)\mathrm{e}{+}42$
MKW4	0.0200	0.186	$1.84^{+0.05}_{-0.03}$	2.00 ± 0.05	$(8.65 \pm 0.24)\mathrm{e}{+}42$	$(8.79 \pm 0.24)\mathrm{e}{+}42$
UGC03957	0.0340	0.459	$\flat 3.19^{+1.36}_{-0.95}$ $\sharp 3.21^{+1.48}_{-1.02}$	1.98 ± 0.19	$(2.49 \pm 0.24)\mathrm{e}{+}43$	$(2.56 \pm 0.25)\mathrm{e}{+}43$
A3827	0.0980	0.284	$\flat 7.55^{+3.21}_{-2.25}$ $\sharp 7.66^{+3.54}_{-2.42}$	1.98 ± 0.19	$(2.10 \pm 0.20)\mathrm{e}{+}44$	$(2.25 \pm 0.22)\mathrm{e}{+}44$
A3822	0.0760	0.212	$5.12^{+0.43}_{-0.31}$	1.98 ± 0.24	$(1.26 \pm 0.15)\mathrm{e}{+}44$	$(1.33 \pm 0.16)\mathrm{e}{+}44$
IIZw108	0.0494	0.663	$\flat 4.25^{+1.81}_{-1.27}$ $\sharp 4.28^{+1.98}_{-1.35}$	1.90 ± 0.23	$(5.06 \pm 0.61)\mathrm{e}{+}43$	$(5.26 \pm 0.63)\mathrm{e}{+}43$
M49	0.0044	0.159	$1.33^{+0.03}_{-0.03}$	1.89 ± 0.03	$(3.93 \pm 0.07)\mathrm{e}{+}41$	$(3.94 \pm 0.07)\mathrm{e}{+}41$
ZwCl1742	0.0757	0.356	$\flat 5.99^{+2.55}_{-1.79}$ $\sharp 6.05^{+2.80}_{-1.91}$	1.87 ± 0.13	$(1.18 \pm 0.08)\mathrm{e}{+}44$	$(1.25 \pm 0.09)\mathrm{e}{+}44$
S405	0.0613	0.765	$\flat 4.98^{+2.12}_{-1.49}$ $\sharp 5.02^{+2.32}_{-1.59}$	1.82 ± 0.24	$(7.48 \pm 1.00)\mathrm{e}{+}43$	$(7.84 \pm 1.05)\mathrm{e}{+}43$
A3532	0.0539	0.596	$4.41^{+0.19}_{-0.18}$	1.78 ± 0.05	$(5.65 \pm 0.17)\mathrm{e}{+}43$	$(5.88 \pm 0.17)\mathrm{e}{+}43$
A3695	0.0890	0.356	$\flat 6.67^{+2.84}_{-1.99}$ $\sharp 6.76^{+3.12}_{-2.14}$	1.76 ± 0.26	$(1.54 \pm 0.23)\mathrm{e}{+}44$	$(1.65 \pm 0.25)\mathrm{e}{+}44$
HCG94	0.0417	0.455	$3.30^{+0.17}_{-0.16}$	1.72 ± 0.03	$(3.25 \pm 0.05)\mathrm{e}{+}43$	$(3.36 \pm 0.06)\mathrm{e}{+}43$
A3528s	0.0551	0.610	$4.60^{+0.49}_{-0.27}$	1.70 ± 0.04	$(5.65 \pm 0.15)\mathrm{e}{+}43$	$(5.89 \pm 0.15)\mathrm{e}{+}43$
S540	0.0358	0.353	$\flat 3.07^{+1.30}_{-0.91}$ $\sharp 3.09^{+1.43}_{-0.98}$	1.62 ± 0.13	$(2.26 \pm 0.18)\mathrm{e}{+}43$	$(2.32 \pm 0.19)\mathrm{e}{+}43$
A2877	0.0241	0.210	$\sharp 3.50^{+2.20}_{-1.10}$	1.61 ± 0.03	$(1.01 \pm 0.02)\mathrm{e}{+}43$	$(1.03 \pm 0.02)\mathrm{e}{+}43$
A3395n	0.0498	0.542	$5.11^{+0.47}_{-0.43}$	1.54 ± 0.10	$(4.16 \pm 0.27)\mathrm{e}{+}43$	$(4.33 \pm 0.28)\mathrm{e}{+}43$
A2151w	0.0369	0.336	$2.58^{+0.19}_{-0.20}$	1.53 ± 0.05	$(2.26 \pm 0.07)\mathrm{e}{+}43$	$(2.33 \pm 0.07)\mathrm{e}{+}43$
A3560	0.0495	0.392	$\flat 3.87^{+1.65}_{-1.15}$ $\sharp 3.90^{+1.81}_{-1.23}$	1.50 ± 0.06	$(4.02 \pm 0.17)\mathrm{e}{+}43$	$(4.17 \pm 0.17)\mathrm{e}{+}43$
A2734	0.0620	0.184	$5.07^{+0.36}_{-0.42}$	1.47 ± 0.06	$(6.19 \pm 0.25)\mathrm{e}{+}43$	$(6.49 \pm 0.26)\mathrm{e}{+}43$
A0548e	0.0410	0.188	$2.93^{+0.17}_{-0.15}$	1.46 ± 0.04	$(2.68 \pm 0.08)\mathrm{e}{+}43$	$(2.77 \pm 0.08)\mathrm{e}{+}43$
A1689	0.1840	0.180	$8.58^{+0.84}_{-0.40}$	1.45 ± 0.03	$(5.53 \pm 0.10)\mathrm{e}{+}44$	$(6.25 \pm 0.11)\mathrm{e}{+}44$
A1914	0.1712	0.097	$8.41^{+0.60}_{-0.58}$	1.45 ± 0.03	$(4.77 \pm 0.11)\mathrm{e}{+}44$	$(5.36 \pm 0.12)\mathrm{e}{+}44$
RXJ2344	0.0786	0.354	$\flat 5.45^{+2.32}_{-1.62}$ $\sharp 5.52^{+2.55}_{-1.74}$	1.37 ± 0.03	$(9.34 \pm 0.21)\mathrm{e}{+}43$	$(9.91 \pm 0.23)\mathrm{e}{+}43$
A3921	0.0936	0.280	$5.39^{+0.38}_{-0.35}$	1.31 ± 0.04	$(1.27 \pm 0.03)\mathrm{e}{+}44$	$(1.36 \pm 0.04)\mathrm{e}{+}44$
A1413	0.1427	0.162	$6.56^{+0.65}_{-0.44}$	1.28 ± 0.03	$(2.92 \pm 0.08)\mathrm{e}{+}44$	$(3.23 \pm 0.09)\mathrm{e}{+}44$

Table 1. continued

NAME	redshift	n_H (10^{21}cm^{-2})	kT_h (keV)	Flux(0.1-2.4keV) $(10^{-11}\text{ergs s}^{-1}\text{ cm}^{-2})$	$^\dagger L_X$ (0.1-2.4keV) $(h^{-2}$ ergs s^{-1} cm$^{-2})$	
					Open	Flat
N5813	0.0064	0.419	$0.76^{+0.19}_{-0.19}$	1.27 ± 0.14	$(5.62 \pm 0.62)\text{e}+41$	$(5.66 \pm 0.62)\text{e}+41$
A1775	0.0757	0.100	$3.66^{+0.34}_{-0.20}$	1.26 ± 0.04	$(8.02 \pm 0.23)\text{e}+43$	$(8.49 \pm 0.25)\text{e}+43$
A3528n	0.0540	0.610	$4.79^{+0.50}_{-0.44}$	1.26 ± 0.05	$(4.00 \pm 0.15)\text{e}+43$	$(4.17 \pm 0.16)\text{e}+43$
A1800	0.0748	0.118	$^\flat 4.95^{+2.11}_{-1.48}$ $^\sharp 5.02^{+2.32}_{-1.59}$	1.20 ± 0.15	$(7.39 \pm 0.95)\text{e}+43$	$(7.82 \pm 1.01)\text{e}+43$
A3888	0.1510	0.120	$^\flat 8.46^{+3.60}_{-2.53}$ $^\sharp 8.68^{+4.01}_{-2.75}$	1.09 ± 0.04	$(2.77 \pm 0.11)\text{e}+44$	$(3.08 \pm 0.12)\text{e}+44$
A3530	0.0544	0.600	$4.05^{+0.32}_{-0.30}$	0.96 ± 0.04	$(3.11 \pm 0.15)\text{e}+43$	$(3.25 \pm 0.15)\text{e}+43$
N5846	0.0061	0.425	$0.64^{+0.04}_{-0.03}$	0.83 ± 0.03	$(3.35 \pm 0.12)\text{e}+41$	$(3.36 \pm 0.12)\text{e}+41$
N499	0.0147	0.525	$0.66^{+0.02}_{-0.03}$	0.45 ± 0.02	$(1.07 \pm 0.04)\text{e}+42$	$(1.08 \pm 0.05)\text{e}+42$
A0548w	0.0424	0.179	$^\flat 1.64^{+0.70}_{-0.49}$ $^\sharp 1.68^{+0.77}_{-0.53}$	0.25 ± 0.02	$(4.84 \pm 0.43)\text{e}+42$	$(5.03 \pm 0.45)\text{e}+42$

$^{*)}$: The Galactic latitude is lower than $20°$.

$^{\dagger)}$: The values are calculated for an open ($\Omega_{m,0} = 0.2$, $\Omega_{\Lambda,0} = 0$) and a flat ($\Omega_{m,0} = 0.2$, $\Omega_{\Lambda,0} = 0.8$) universe.

$^{\flat)}$: The temperature is estimated with the $L - T$ relation assuming the open universe.

$^{\sharp)}$: The temperature is estimated with the $L - T$ relation assuming the flat universe.

$^{\natural)}$: The temperature is derived with non-*ASCA* spectroscopy. *Einstein* MPC for A2877 and A1644 (David et al. 1993), *EXOSAT* LE+ME for EXO0422 (Edge & Stewart 1991), and *XMM-Newton* EPIC for S1101 (Kaastra et al. 2001).

Table 3. Fitting Results

Model XTF	$\Omega_{m,0}$	σ_8	A	α	$\sigma_{\log L}$
PS(Open)	$0.18^{+0.08}_{-0.05}$	$0.96^{+0.11}_{-0.09}$	$42.15^{+0.17}_{-0.20}$	$2.47^{+0.26}_{-0.24}$	$0.24^{+0.04}_{-0.04}$
PS(Open,$T > 3$keV)	$0.25^{+0.12}_{-0.09}$	$0.89^{+0.13}_{-0.11}$	$42.19^{+0.27}_{-0.37}$	$2.42^{+0.38}_{-0.37}$	$0.22^{+0.05}_{-0.03}$
FE(Open,s=0)	$0.15^{+0.07}_{-0.05}$	$0.98^{+0.08}_{-0.07}$	$42.14^{+0.17}_{-0.20}$	$2.49^{+0.26}_{-0.25}$	$0.24^{+0.04}_{-0.04}$
FE(Open,s=1)	$0.11^{+0.07}_{-0.05}$	$0.68^{+0.04}_{-0.03}$	$42.12^{+0.18}_{-0.20}$	$2.51^{+0.27}_{-0.25}$	$0.24^{+0.04}_{-0.04}$
PS(Flat)	$0.19^{+0.08}_{-0.05}$	$1.02^{+0.12}_{-0.11}$	$42.15^{+0.17}_{-0.20}$	$2.49^{+0.26}_{-0.25}$	$0.24^{+0.04}_{-0.03}$
PS(Flat,$T > 3$keV)	$0.26^{+0.12}_{-0.09}$	$0.94^{+0.14}_{-0.13}$	$42.19^{+0.27}_{-0.29}$	$2.44^{+0.39}_{-0.38}$	$0.23^{+0.04}_{-0.04}$
FE(Flat,s=0)	$0.18^{+0.07}_{-0.05}$	$1.14^{+0.13}_{-0.11}$	$42.15^{+0.17}_{-0.20}$	$2.49^{+0.26}_{-0.25}$	$0.24^{+0.04}_{-0.03}$
FE(Flat,s=1)	$0.14^{+0.06}_{-0.05}$	$0.89^{+0.08}_{-0.08}$	$42.14^{+0.17}_{-0.21}$	$2.51^{+0.26}_{-0.25}$	$0.24^{+0.04}_{-0.03}$

– The error ranges corresponding to 90% confidence for one parameter of interest.